Multiconfiguration Dirac-Hartree-Fock theory for copper $K\alpha$ and $K\beta$ diagram lines, satellite spectra, and *ab initio* determination of single and double shake probabilities

T. V. B. Nguyen,[*] H. A. Melia,[†] F. I. Janssens,[‡] and C. T. Chantler[§]
School of Physics, The University of Melbourne, Melbourne, Australia

(Received 24 November 2021; accepted 7 January 2022; published 14 February 2022)

The x-ray spectra of copper $K\alpha$ and $K\beta$ remain a topic of great interest due to the complex open-shell processes involved, with many discrepancies among theories and experiments. We present high-accuracy theory of copper $K\alpha$ and $K\beta$ diagram and satellite spectra in the multiconfiguration Dirac-Hartree-Fock method. Diagram spectra are expanded to $5s$ with simultaneous convergence of 28 000 configuration state functions (CSFs) ($K\alpha$) and to $6g$ with simultaneous convergence of 91 000 CSFs ($K\beta$), achieving eigenvalue convergence to ± 0.03 eV or 0.000 25%, approximately a factor of 10 improvement over past work. It is necessary to invoke biorthogonalization, developments of the active space approach, analysis of markers for theoretical convergence of eigenvalues, and the question of self-consistency for both $K\alpha$ and $K\beta$ spectra. We make use of gauge convergence, eigenvalue convergence, and A-coefficient convergence. The satellite spectra are a major outcome—without these, it is not possible to make use of the increased accuracy of the diagram computations. The Cu $K\alpha$ $3d^8$ double shake satellite spectrum alone contains 1506 unique eigenvalues (transitions) and required simultaneous convergence of 593 000 CSFs. *Ab initio* shakeoff probabilities for $1s$, $2s$, $2p$, $3s$, $3p$, $3d$, and $4s$ subshells as a result of the K-shell photoionization process are presented. Portable spectral representations are provided in the supplemental material, discussed in the text. We investigate the meaning behind shake, shakeoff, and shakeup processes and the computational potential to investigate these at the current time. We separate the notions of total shake, single shake, and double shake, explain how these are observable in high-quality experimental spectra, and how these calculations can be used experimentally.

DOI: 10.1103/PhysRevA.105.022811

I. INTRODUCTION

An understanding of characteristic radiation due to inner-shell processes of open-shell systems is vital across many research disciplines, spanning from medical [1] to fusion studies [2]. The most intense and widely used x-ray emission line is the $K\alpha$ transition, which features prominently in many laboratory-based experiments [3–5], and in much astrophysical research, such as probing galactic variabilities [6] and diagnosing black hole spin [7]. Despite its multitudinous applications, the structure of $K\alpha$ photoemission spectra, and that of its closest relative, $K\beta$, are among the longest-running unsolved open-shell challenges in atomic physics. Open-shell systems are notoriously complex, demanding some of the most advanced theoretical framework to model, and even then success is not guaranteed. The last high-accuracy theoretical work on copper $K\alpha$ was carried out about a decade ago [8], employing advanced relativistic techniques to obtain some of the best results at the time. However, computational constraints permitted only a partial set of results, with further approximations required to complete the set. The latest high-accuracy theoretical work on copper $K\beta$ was published in 2016 [9]. This overcame the earlier challenges and was able to obtain a full set of spectra, yet other approximations had to be made to obtain convergence [9]. Herein, we use one of the most advanced relativistic atomic theories and computational frameworks available for the computation of copper $K\alpha$ and $K\beta$ spectra within a uniform approach. This work obtains a complete set of spectra, achieving a high degree of convergence while avoiding the earlier approximations [8,9]. Consequently, these results are much more robust with high accuracy, probing further into the characteristic spectra.

The primary $K\alpha$ process involves an electronic transition from the $1s^1\,2s^2\,2p^6$ core (or $1s^{-1}$ for short) to the $1s^2\,2s^2\,2p^5$ core (or $2p^{-1}$). Under the jj-coupling scheme, the $2p$ subshell is split into two levels: $2p_{1/2}$ and $2p_{3/2}$. The energy separation depends on relativistic effects. In a simplistic framework, the $K\alpha$ inner-shell photoemission spectrum would be composed of a few primary diagram lines derived from relativistic quantum theory—corresponding to transitions from $2p_{3/2}$ ($K\alpha_1$) or $2p_{1/2}$ transitions ($K\alpha_2$). Similarly, the $K\beta$ spectrum is a result of the electronic transition $1s^{-1} \rightarrow 3p^{-1}$, where the $3p$ subshell is also split into two levels, $3p_{3/2}$ and $3p_{1/2}$. $1s^{-1} \rightarrow 3p_{3/2}^{-1}$ is $K\beta_1$, whereas $1s^{-1} \rightarrow 3p_{1/2}^{-1}$ is $K\beta_3$. While the copper $K\alpha$ spectrum shows two distinctive peaks as a result of the primary diagram lines arising from the $2p_{1/2}$ and $2p_{3/2}$ transitions, the $K\beta$ diagram lines are extremely close together, unresolved with present technology. Analysis of copper $K\beta$ requires highly accurate theoretical calculations as a tool to overcome the resolution challenge. Copper

[*]b.nguyen6@student.unimelb.edu.au
[†]hmelia@student.unimelb.edu.au
[‡]fjanssens@student.unimelb.edu.au
[§]Corresponding author: chantler@unimelb.edu.au

$K\alpha$ and $K\beta$ spectra are asymmetric [10], beyond the simple bound-bound diagram transitions. There are other transitions involved across the energy spectrum, commonly referred to as satellite lines.

Many theories have attempted to explain the additional structure and asymmetry [11–13]. The interpretation that the satellite lines are caused by shake processes [14] is the most prominent and widely accepted view. Following the ionization of a core $1s$ electron by x-rays, the outer-shell electrons are no longer in the eigenstate of the atom, and additional electrons might be shaken up or ejected. Then, when a $2p$ electron decays to the $1s$ level, the spectrum might have already shifted relative to the diagram lines. The photoionization of the $1s$ electron may result in the ejection of an additional electron into the continuum (shakeoff). A popular model for shake processes is the sudden approximation model. This proposes that in the high-energy limit, the initial ionization and subsequent shake processes occur within a much shorter time frame than the relaxation time. Consequently, the orbital relaxation results in transition lines in addition to the diagram lines.

It is important to understand all the processes and transitions involved with the copper x-ray spectrum, especially for high-accuracy investigations. The complexity of the additional shake processes must be investigated. There are large discrepancies between *ab initio* calculations of shakeoff probabilities and experimental results. Groundbreaking work on copper $K\alpha$ on both theory and experiment was performed by Deutsch *et al.* in the 1990s [10]. However, there were some limitations due to the lack of computational resources [15,16]. One of the major approximations made was to ignore the $4s$ electron, which effectively treated the copper atom as a closed-shell problem. This significantly simplified the computational challenge, resulting in an accuracy of perhaps 1–2 eV. Later work [15] has claimed an accuracy level <0.1 eV by including the $4s$ as well as transforming two nonorthogonal basis sets into a single biorthogonal set, allowing for the calculation of transition matrix elements. Now, further improvements have been developed, allowing for more highly accurate calculations with fewer approximations.

II. THEORY AND CALCULATIONS

Atomic wave functions are calculated using the multiconfiguration Dirac-Hartree-Fock (MCDHF) method, implemented computationally by GRASP2K, a fully relativistic atomic structure package [17]. *Ab initio* shakeoff probabilities and relativistic atomic wave functions are generated using a modified version of the GRASP2K package [18] built upon a QED ansatz [19], verified to be consistent with some of the best experimental data available [20]. Breit [21] and QED effects [19] are added perturbatively, which presents no limitation compared with incorporating these effects at the self-consistent stage of calculation [21]. The MCDHF method is an extension to the relativistic Dirac-Hartree-Fock (DHF) method for many-electron systems. The widely known single-configuration DHF method requires solving a single determinant as a solution to the usual central field problem, whereas the multiconfiguration framework demands a linear combination of determinants as a solution to the problem. Thus, the total wave function, or the atomic state function (ASF), is a linear combination of configuration state functions (CSFs):

$$\Psi_{E\kappa m} = \sum_q c_q \, \Phi_{qE\kappa m}(\mathbf{r}), \tag{1}$$

where c_q is the mixing coefficient which can be found by diagonalizing the Dirac-Coulomb Hamiltonian,

$$H_{\mathrm{DC}} = \sum_i^N \left\{ c\,\boldsymbol{\alpha_i}\cdot\boldsymbol{p_i} + \beta_i mc^2 + V_{\mathrm{nuc}}(r_i) + \sum_{i<j}^N \frac{1}{r_{ij}} \right\}, \tag{2}$$

for an N-electron system. Each CSF, Φ, is an antisymmetrized determinant built from single electronic Dirac central field orbitals,

$$\phi_{E\kappa m} = \frac{1}{r}\begin{pmatrix} P_{E\kappa}(r)\chi_{\kappa m}(\theta,\varphi) \\ iQ_{E\kappa}(r)\chi_{-\kappa m}(\theta,\varphi) \end{pmatrix}, \tag{3}$$

which contains all the necessary information such as quantum numbers and parity, $E\kappa m$, to distinguish between the different states. P and Q are the complex radial wave function, and χ is the angular wave function for each component. Formally, GRASP2K uses the development of Racah algebra using quasi-spin space to aid in the orthogonalization, particularly of f-states compared with the more simple, older, Slater operation, for the spin-angular-momentum parts of the wave function and matrix elements [22,23].

A single configuration calculation where we only use the first-order, base electronic structure of copper, namely $1s^2\,2s^2 2p^6\,3s^2 3p^6 3d^{10}\,4s^1$, yields a decent approximate result, perhaps to 1 eV accuracy, but insufficient for the purpose of high-accuracy investigations. Hence, various possible configurations are combined with the base configuration to build up a more complete wave function—a multiconfiguration approach. Our higher-order configuration expansions are obtained using the active-space approach, where the CSFs are generated by single or double excitations from the reference (first-order) configuration to an active set of orbitals. Double excitations allow for correction of deficiencies within the radial wave function and to account for electron-electron correlation. Triple excitations can account for electron-electron-electron correlation, yet these higher-order effects are extremely small [24,25] and not included in the present calculations. The active set should be expanded in a systematic way, yet the method of expansion can greatly affect the system in question. In addition to the transition energies, Einstein A-coefficients are calculated. Results can be obtained in both relativistic length and velocity gauges (Babushkin and Coulomb gauges). More detailed discussions of the MCDHF framework can be found in advanced relativistic atomic texts [26]. Details specific to the theoretical approach presented here can be found in [8,9,24].

A. Methodology for $K\alpha$ calculations

Our method involves sequentially expanding the reference configuration, while also keeping the inner core of $n = 1, 2$ effectively frozen or inactive. Two separate atomic states were built: the "initial" state with $1s^1\,2s^2\,2p^6$, and a "final" state with $1s^2\,2s^2\,2p^5$ to emulate the $K\alpha$ transition. This captures the wave function just after the copper atom has

been ionized with the removal of the $1s$ electron. For general advanced computation methods, it has become essential to invoke biorthogonalization, as in GRASP2K, when the scalar product of vectors formed is a linear combination of two sets of linearly independent vectors, e.g., for overlap probabilities. If one wants the scalar product to have the usual form, the two sets of basis vectors should be biorthogonal. The maximum total angular momentum number, J, was restricted to a set of values determined from the dominant single configuration. More explicitly, $J_{\text{initial}} \in \{0, 1\}$ and $J_{\text{final}} \in \{0, 1, 2\}$ for all cases, even after expansion to the multiconfiguration level. Thus, the number of diagram transitions is restricted to 6. If all possible excitations to the active set are allowed, we would have a complete active space. A complete active space for few-electron atoms is feasible but for copper is computationally infeasible. Just after ionization, this would demand all possible configurations of 28 electrons.

In our calculations, we expanded our active set up to $5s$. There is always a tradeoff between computation time and accuracy. As we expand our active set $n \to \infty$, the atomic wave function should approach completeness. Moreover, there is no single, general recipe for all atomic systems that guarantees fast and stable convergence. For Cu $K\alpha$ calculations, holding the $1s\,2s\,2p$ subshells frozen at the multiconfiguration level and expanding by principal quantum number leads to a fast and stable convergence of results. After an expansion up to $4f$, an additional expansion to the $5s$ level makes little difference to energy levels and convergence of the two gauges. This has been used as a proxy signal that our results have reached a sufficiently high level of convergence.

B. Methodology for $K\beta$ calculations

The procedures for calculating the Cu $K\beta$ spectrum is similar to $K\alpha$. For the purpose of demonstrating some challenges encountered with open-shell atomic transition calculations, three alternative methods for calculating Cu $K\beta$ are presented. For Method 1, we have adopted the same procedure as for the Cu $K\alpha$ calculations. That is, we hold the subshells $1s\,2s\,2p$ inactive while systematically expanding the active space. In Method 2, we kept only the $1s$ and $3p$ subshells inactive, while the rest were active. Finally, in Method 3 we hold all subshells between $1s$ and $3p$ inactive. The common rationale among all three methods in freezing the $1s$ shell is to provide added stability at the core level where the primary $K\beta$ transition would occur. The maximum total angular momentum number, J, was restricted in the same fashion as those of $K\alpha$ calculations, yielding a total of six possible $K\beta$ diagram transitions. In the recent work of Cu $K\beta$ [9], the method employed was similar to Method 1. However, the authors encountered some difficulties, namely false convergence, and at times nonconvergence, requiring manual selection and ordering of dominant CSFs in order to achieve reasonable convergence. We will demonstrate this false convergence [9], as well as a more robust solution that does not require manual selection of the CSFs.

C. *Ab initio* shake probabilities using the sudden approximation

Initially the atom is in the neutral ground state, with a wave function $\Psi_A(N+1)$ being an eigenstate of the $N+1$ Hamiltonian. The removal of a $1s$ electron causes a transformation in the wave function $\Psi_A(N+1) \to \tilde{\Psi}_A(N)$. The wave function of the N-electron system is the same wave function as the neutral $N+1$ system except with one missing electron (single-electron wave functions are the same for both systems, but not the normalized atomic wave function). This is valid in the high-energy limit because the wave function does not have enough time to adjust. Upon relaxation, the transformation $\tilde{\Psi}_A(N) \to \Psi_B(N)$ occurs, where the $\Psi_B(N)$ wave function represents the relaxed $1s^{-1}$ atom. Under the sudden approximation [27–29], the probability of finding the atom in the stable $1s$ hole state, $|\Psi_B\rangle$, given that it was originally in the $|\tilde{\Psi}_A\rangle$ state, is

$$P = |\langle \Psi_B(N) | \tilde{\Psi}_A(N) \rangle|^2. \tag{4}$$

The probability of shakeup or shakeoff occurring is then the probability of finding the atom in any other state:

$$P_{\text{total}}^{\text{shake}} = 1 - |\langle \Psi_B(N) | \tilde{\Psi}_A(N) \rangle|^2. \tag{5}$$

By substitution using Eq. (1), we can write this as

$$P_{\text{total}}^{\text{shake}} = 1 - \left| \sum_j \sum_k c_j d_k \, \langle \Phi_{Bk}(N) | \tilde{\Phi}_{Aj}(N) \rangle \right|^2. \tag{6}$$

Here j runs over each of the CSFs that make up the initial-state wave function, and k runs through each of the CSFs that make up the final-state wave function. Each of these individual CSFs can be written in terms of a product of antisymmetrized single-electron determinants:

$$\Phi_{En\kappa} = \mathcal{A}\left[\prod_{i=1}^{N} \phi_{iEn\kappa}(\mathbf{r}) \right], \tag{7}$$

$$|\Phi_{An\kappa}\rangle = \mathcal{A} \prod_{i=1}^{N} |\phi_{iAn\kappa}\rangle\,, \quad |\Phi_{Bn\kappa}\rangle = \mathcal{A} \prod_{i=1}^{N} |\phi_{iBn\kappa}\rangle\,, \tag{8}$$

where n is the principal quantum number and κ is the relativistic quantum number: $\kappa = \mp(j + \frac{1}{2})$ for $j = \ell \pm \frac{1}{2}$. The antisymmetrizing operator $\mathcal{A}$ is defined using the permutation operator $\hat{\mathcal{P}}$:

$$\mathcal{A} = \frac{1}{N!} \sum_{P \in S_N} (-1)^{\pi} \hat{\mathcal{P}}, \tag{9}$$

where P is a permutation in the set of N-element permutations S_N, and π is the number of independent permutation exchanges of particles. As $\mathcal{A}^\dagger = \mathcal{A}$ and $\hat{\mathcal{P}}\hat{\mathcal{P}}^\dagger = 1$, we can rewrite the overlap in Eq. (6) as

$$\langle \Phi_{Bk}(N) | \tilde{\Phi}_{Aj}(N) \rangle = \left\langle \prod_{n'\kappa'} \phi_{Bkn'\kappa'} \middle| \prod_{n\kappa} \tilde{\phi}_{Ajn\kappa} \right\rangle. \tag{10}$$

Under the assumption that inner-shell photoionization includes only shakeoff processes, any subshells with different quantum numbers, n and κ, have zero overlap:

$$\langle \phi_{Bkn'\kappa'} | \tilde{\phi}_{Ajn\kappa} \rangle = \begin{cases} 0 & \text{for } n \neq n', \quad \kappa \neq \kappa', \\ (1 - \epsilon_{n\kappa}) & \text{for } n = n', \quad \kappa = \kappa';\ \epsilon_{n\kappa} = 1 - \langle \phi_{Bkn\kappa} | \tilde{\phi}_{Ajn\kappa} \rangle\,. \end{cases} \tag{11}$$

For excitation energies well above threshold, this has been shown to be a good assumption [30–32]. Using this, we can simplify the double product in Eq. (10) to

$$\langle \Phi_{Bk}(N)|\tilde{\Phi}_{Aj}(N)\rangle = \prod_{n\kappa} \langle \phi_{Bkn\kappa}|\tilde{\phi}_{Ajn\kappa}\rangle^{M_{n\kappa}}, \tag{12}$$

where $M_{n\kappa}$ is the number of electrons with quantum numbers $n\kappa$. Substituting this into Eq. (6) gives the total shake probability, P_{shake}, as

$$P_{\text{total}}^{\text{shake}} = 1 - \left| \sum_j \sum_k c_j d_k \prod_{n\kappa} \langle \phi_{Bkn\kappa}|\tilde{\phi}_{Ajn\kappa}\rangle^{M_{n\kappa}} \right|^2 = 1 - \left| \sum_j \sum_k c_j d_k \prod_{n\kappa} (1-\epsilon_{n\kappa})^{M_{n\kappa}} \right|^2. \tag{13}$$

The next step involves the following three Taylor series expansions, each to first order:

$$(1-\epsilon_{n\kappa})^{M_{n\kappa}} \approx (1 - M_{n\kappa}\epsilon_{n\kappa}), \quad \left| \sum_j \sum_k c_j d_k \prod_{n\kappa} (1 - M_{n\kappa}\epsilon_{n\kappa}) \right|^2 \approx \left| \sum_{jj'kk'} c_j d_k c_{j'} d_{k'} \prod_{n\kappa} (1 - 2M_{n\kappa}\epsilon_{n\kappa}) \right|,$$
$$\prod_{n\kappa} (1 - 2M_{n\kappa}\epsilon_{n\kappa}) \approx 1 - \sum_{n\kappa} 2M_{n\kappa}\epsilon_{n\kappa}. \tag{14}$$

Combining these and applying them to Eq. (13) gives

$$\begin{aligned} P_{\text{total}}^{\text{shake}} &\approx 1 - \left| \sum_j \sum_k c_j d_k \prod_{n\kappa} (1 - M_{n\kappa}\epsilon_{n\kappa}) \right|^2 \\ &\approx 1 - \left| \sum_{jj'kk'} c_j d_k c_{j'} d_{k'} \prod_{n\kappa} (1 - 2M_{n\kappa}\epsilon_{n\kappa}) \right| \\ &\approx 1 - \left| \sum_{jj'kk'} c_j d_k c_{j'} d_{k'} \left(1 - \sum_{n\kappa} 2M_{n\kappa}\epsilon_{n\kappa} \right) \right|. \end{aligned} \tag{15}$$

We can expand the last line of Eq. (15), and the first two terms combine to approximately zero. Therefore, we can make the approximation

$$\begin{aligned} P_{\text{total}}^{\text{shake}} &= \underbrace{1 - \sum_{jj'kk'} c_j d_k c_{j'} d_{k'}}_{\approx 0} \\ &\quad - \sum_{n\kappa} \sum_{jj'kk'} c_j d_k c_{j'} d_{k'} 2M_{n\kappa}\epsilon_{n\kappa}, \end{aligned}$$

$$1 - \sum_{jj'kk'} c_j d_k c_{j'} d_{k'} \approx \sum_{n\kappa} \left(1 - \sum_{jj'kk'} c_j d_k c_{j'} d_{k'} \right). \tag{16}$$

Applying this approximation to the last line of (15) gives

$$\begin{aligned} P_{\text{total}}^{\text{shake}} &\approx \sum_{n\kappa} \left(1 - \sum_{jj'kk'} c_j d_k c_{j'} d_{k'} \right) \\ &\quad - \sum_{n\kappa} \sum_{jj'kk'} c_j d_k c_{j'} d_{k'} 2M_{n\kappa}\epsilon_{n\kappa}, \\ P_{\text{total}}^{\text{shake}} &\approx \sum_{n\kappa} \left(1 - \sum_{jj'kk'} c_j d_k c_{j'} d_{k'} - \sum_{jj'kk'} c_j d_k c_{j'} d_{k'} 2M_{n\kappa}\epsilon_{n\kappa} \right), \\ P_{\text{total}}^{\text{shake}} &\approx \sum_{n\kappa} \left(1 - \sum_{jj'kk'} c_j d_k c_{j'} d_{k'} \left(1 - 2M_{n\kappa}\epsilon_{n\kappa}\right) \right). \end{aligned} \tag{17}$$

Similar to Eq. (14), consider the following two reversed Taylor series expansions:

$$\sum_{jj'kk'} c_j d_k c_{j'} d_{k'} (1 - 2M_{n\kappa}\epsilon_{n\kappa}) \approx \left| \sum_j \sum_k c_j d_k (1 - M_{n\kappa}\epsilon_{n\kappa}) \right|^2,$$
$$(1 - M_{n\kappa}\epsilon_{n\kappa}) \approx (1 - \epsilon_{n\kappa})^{M_{n\kappa}}. \tag{18}$$

Applying these to the last line of Eq. (17) gives

$$\begin{aligned} P_{\text{total}}^{\text{shake}} &\approx \sum_{n\kappa} \left| 1 - \sum_j \sum_k c_j d_k \left(1 - \epsilon_{n\kappa}\right)^{M_{n\kappa}} \right|^2 \\ &= \sum_{n\kappa} \left| 1 - \sum_j \sum_k c_j d_k \, \langle \phi_{Bkn\kappa}|\phi_{Ajn\kappa}\rangle^{M_{n\kappa}} \right|^2 \\ &= \sum_{n\kappa} P_{n\kappa}^{\text{shake}}. \end{aligned} \tag{19}$$

We now have the total shake probability as a sum of shake probabilities for each $n\kappa$ subshell. The probability of electron shakeoff from subshell $n\kappa$ is given by

$$P_{n\kappa}^{\text{shake}} = 1 - \left| \sum_j \sum_k c_j d_k \, \langle \phi_{Bkn\kappa}|\phi_{Ajn\kappa}\rangle^{M_{n\kappa}} \right|^2. \tag{20}$$

Because the states are orthogonal, the double sum can be reduced to a single sum. Furthermore, because the wavefunction components P and Q are independent of j, the overlap $\langle \phi_{Bjn\kappa}|\phi_{Ajn\kappa}\rangle$ is a constant, and the j index can be removed. Although the overlap does not depend on which CSF we are considering, the occupation number of the $n\kappa$ subshell may be different for different CSFs, so the overlap must remain inside the sum over j. This has been made explicit by subscripting the occupation number with j:

$$P_{n\kappa}^{\text{shake}} = 1 - \left| \sum_j c_j d_j \, \langle \phi_{Bn\kappa}|\phi_{An\kappa}\rangle^{M_{jn\kappa}} \right|^2. \tag{21}$$

This is similar to the nonrelativistic analog of Carlson *et al.* [28] and Mukoyama and Taniguchi [29],

$$P_{nl}^{\text{shake}} = 1 - (|\langle\phi_{Bnl}|\phi_{Anl}\rangle|^2)^{M_{nl}} - P_F, \tag{22}$$

where P_F represented forbidden transitions where the upper state is (already) occupied. Using Eqs. (20) and (21), we have calculated each of the vacancy state probabilities in the following sections, with $M_{jn\kappa}$ being the occupation number of the $n\kappa$ state in the jth CSF. It is often useful to have this in the form of probability per electron, $p_{n\kappa}$:

$$p_{n\kappa} = \frac{1}{M_{n\kappa}}\left(1 - \left|\sum_j c_j d_j \langle\phi_{Bn\kappa}|\phi_{An\kappa}\rangle^{M_{jn\kappa}}\right|^2\right). \tag{23}$$

The overlap of the orbital radial wave functions in Eq. (21) is

$$\langle\phi_{Bn\kappa}|\phi_{An\kappa}\rangle = \int_0^\infty (P_{B\kappa}P_{A\kappa} + Q_{B\kappa}Q_{A\kappa})\, dr, \tag{24}$$

where dr is specific to the grid of the theory employed. In this case, dr is defined as $(r_{i+1} - r_{i-1})/2$. The ϕ's represent the radial wave functions of the ground-state (or neutral) copper atom and its ionized state immediately after the removal of the $1s$ electron. The mixing coefficients of the two states are represented by c_j and c_k. This equation describes the shakeoff probability in the high-energy (sudden approximation) limit. Given that the copper atom is initially assumed to be in a state represented by $1s^2\,2s^2\,2p^6$, after the photoionization process where the configuration becomes $1s^1\,2s^2\,2p^6$, what is the probability that the orbitals actually relax to the $1s^1\,2s^2\,2p^6$ state? The squared term in Eq. (6) seeks to represent such a probability. Consequently, when this probability is subtracted from unity, what remains is the probability that the atom did *not* relax to the $1s^1\,2s^2\,2p^6$ state, i.e., a shake probability. Equation (20) describes the probability that an event has occurred where an electron is shaken off from subshell n, κ immediately after the photoionization but before orbital relaxation could occur (sudden approximation), and thus the atom would relax to a state configuration other than $1s^1\,2s^2\,2p^6$. All the inputs required by Eq. (20) are extracted from GRASP2K calculations.

In previous work we utilized about 200 mixing coefficients and electronic configurations [9]; however, in this study we have used all available configurations. To accomplish this task, the mixing coefficients for both states and their corresponding electronic configurations had to be ordered and aligned with each other. Without doing so, one would certainly risk mismatching the mixing coefficients and their corresponding CSFs between the two states, which means that Eq. (20) would be applied incorrectly. Once the coefficients are ordered and matched correctly, they are normalized and used to calculate the final shakeoff probabilities. The normalization process requires the summation of the mixing coefficients to be divided by the normalization factor,

$$\text{Normalization factor} = \sqrt{\sum_j^N c_j^2 \sum_k^N d_k^2}, \tag{25}$$

where N is the number of mixing coefficients used. In principle, if all the mixing coefficients and configuration state functions are used in the calculation, the normalization factor would be unity and its inclusion would not alter the results. However, depending on the type of transition in which we are interested, it is not always possible to match up all the configuration state functions and their corresponding mixing coefficients, in which case a normalization factor should be included.

III. Cu $K\alpha$ CHARACTERISTIC EIGENVALUES AND AMPLITUDES

Table I presents the results for the $K\alpha$ diagram eigenvalues. Gauge convergence in atomic structure calculations is a necessary but insufficient condition for accuracy. We use it as a monitor on the quality and convergence of results. Even with the single configuration calculations where only the first-order term was used (no correlation), the gauges have converged quite well to within less than a percent of unity. Further expansion to $4f$ and $5s$ shows that there is little variation in the gauge ratio. This is an indicator that the wave

TABLE I. Calculated results of copper $K\alpha$ diagram transitions, where the results of the single configuration as well as expansion up to $4f$ and $5s$ are included. At the $5s$ level, almost 28 000 CSFs were deployed. The ratio A^L/A^V is the gauge ratio between the relativistic length (Babushkin) and velocity (Coulomb) gauges. A ratio that is close to unity is indicative of a high degree of gauge invariance, which also serves as one of the proxy indicators of the level of convergence of the calculated results. The numbers in parentheses are the difference between the current expansion compared to the previous one, which we have used as an approximation of the errors as well as an indicator of convergence. The g_f values in Coulomb gauge are also provided, which yields an $I(K\alpha_2) : I(K\alpha_1)$ ratio of 0.5115. The full spectrum expanded to $5s$ is included in text form in the Supplemental Material [33] as Kaicu-5s.fcu-5s.ct.

	Single configuration		Expansion to $4f$		Expansion to $5s$			Chantler *et al.* [8]
Transition	Energy (eV)	A^L/A^V	Energy (eV)	A^L/A^V	Energy (eV)	A^L/A^V	g_f	Energy (eV)
$K\alpha_1$								
$J=0 \to J=1$	8047.17	1.0065	8047.92 (±0.75)	1.0067	8047.90 (±0.02)	1.0067	0.214935	8048.09
$J=1 \to J=1$	8047.07	1.0065	8047.83 (±0.76)	1.0067	8047.80 (±0.03)	1.0067	0.108004	8047.88
$J=1 \to J=2$	8047.16	1.0065	8047.86 (±0.70)	1.0067	8047.84 (±0.02)	1.0067	0.538166	8047.88
$K\alpha_2$								
$J=0 \to J=1$	8027.11	1.0067	8028.01 (±0.90)	1.0070	8027.99 (±0.02)	1.0069	0.110581	8028.18
$J=1 \to J=0$	8027.05	1.0067	8027.94 (±0.89)	1.0069	8027.92 (±0.02)	1.0069	0.109988	8027.95
$J=1 \to J=1$	8027.01	1.0067	8027.93 (±0.92)	1.0069	8027.90 (±0.03)	1.0069	0.219854	8027.95

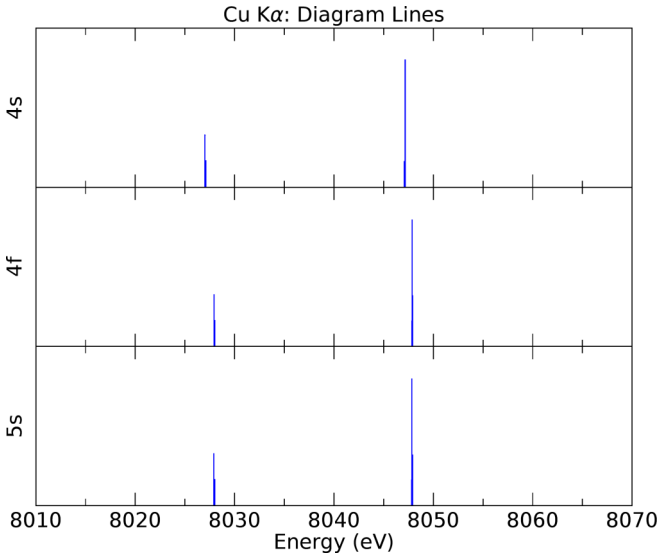

FIG. 1. Demonstration of the convergence of the eigenvalues of the Cu $K\alpha$ diagram spectrum with expansion to outer orbitals.

function constructed from the start was robust and stable. The gauge discrepancy is almost constant for all observed spectral components, meaning that any relative g_f structural variation of components between gauges lies around 0.02% rather than the gauge convergence level of 0.6–0.7 %.

The expansion from the single configuration ($4s$) to the ($4f$) multiconfiguration level shows a change in energy of almost 1 eV, even while the gauge ratios are stable. Between the $4f$ and $5s$ expansions, the energies did not change very significantly and the gauge ratios hardly changed at all. This is indicative of a satisfactory gauge and energy convergence (Fig. 1). Further expansion would add hundreds of thousands of additional higher-order terms (CSFs). We have included the change in energy from one expansion to the next as an error estimation, given in the parentheses. Table I illustrates the change in energy from the $4s$ (single configuration SCF) stage to the $4f$ multiple configuration expansion. The changes in energy for $K\alpha_1$ are consistently around 0.70 eV, while those for $K\alpha_2$ are around 0.90 eV. Although all transitions eventually exhibit a similar change in energy by the $5s$ stage, the initial results appear to suggest that $K\alpha_2$ transitions may suffer a higher instability than those of $K\alpha_1$ when insufficient CSFs are used. This may be related to the difference between the $2p_{1/2}$ and $2p_{3/2}$ levels. Energies, gauges, and the g_f values in the Coulomb gauge for our final set of results ($5s$) are provided.

The energies are provided in units of cm^{-1}, converted to eV using the 2018 CODATA recommended values [34]. The eigenvalues presented here are generally smaller than [8] by around 0.03–0.19 eV, or around the anticipated accuracy of the previous work. Reference [8] did not calculate the full set of diagram lines simultaneously due to the difficulty in obtaining convergence when handling a large basis set. Consequently, the authors only calculated a few primary lines to a high level of accuracy and then scaled the rest accordingly. In this current work, all the diagram lines have been obtained simultaneously using the same basis set, and thus are likely to be more accurate than the earlier approximations [8]. Our intensity ratio for the theoretical diagram lines $I(K\alpha_2)/I(K\alpha_1)$ is 0.5115, which is slightly lower than a much earlier theoretical determination of 0.513 by Scofield [35], including exchange interactions but not satellite contributions. If we define an uncertainty by the variation from different expansions, we may estimate a diagram line ratio of 0.5115 ± 0.0015.

Experimental fits of Hölzer *et al.* [36] report total spectra including satellites and experimental ratios of $I(K\alpha_2)/I(K\alpha_1) = 0.518(20)$, whereas Mendenhall *et al.* [37] reported 0.520 00(22) in their Table IV, and 0.518 and 0.521 in their Table V, comparing data from different years. Hölzer *et al.* discuss the consistency with earlier experimental interpretations of Williams [38], Salem *et al.* [39,40], and McGrary *et al.* [41], which obtained experimental results from 0.498 to 0.508 and 0.512(10), respectively [36]: "A more serious problem for the accurate determination of $I(K\alpha_2)/I(K\alpha_1)$ is the partitioning of the intensity of the spectrum between the two lines. The intensity between the doublet lines is nonzero and thus its assignment is done using additional assumptions, such as an identical peak shape or a fixed ratio of the FWHM of the doublet peaks [41]. These assumptions are not universally valid, particularly in these cases where the shapes of the $K\alpha_1$ and the $K\alpha_2$ peaks are significantly different." These comments remain fully valid and at this point are indicative of consistency of theory without addressing the meaning of experimental variation (see the Conclusion).

TABLE II. Copper $K\beta$ diagram lines using Method 1 where subshells $1s\,2s\,2p$ are frozen while the rest are active. The eigenvalues are clearly wrong, and the convergence level between the gauges has deteriorated at the first multiconfiguration expansion level to $4f$. By the $4f$ stage using Method 1, just over 13 000 CSFs were used for the calculation.

	Single configuration		Expansion to $4f$	
Transitions	Energy (eV)	A^L/A^V	Energy (eV)	A^L/A^V
$K\beta_1$				
$J=0 \rightarrow J=1$	8902.76	1.0062	8953.92	1.0186
$J=1 \rightarrow J=1$	8902.67	1.0063	8953.84	1.0186
$J=1 \rightarrow J=2$	8902.92	1.0063	8954.15	1.0187
$K\beta_3$				
$J=0 \rightarrow J=1$	8900.31	1.0065	8951.01	1.0179
$J=1 \rightarrow J=0$	8900.36	1.0066	8950.71	1.0179
$J=1 \rightarrow J=1$	8900.21	1.0066	8950.92	1.0179

IV. Cu $K\beta$ CHARACTERISTIC EIGENVALUES AND AMPLITUDES

Three methods of calculation are deployed for Cu $K\beta$ (Tables II, III, and IV). While the idea of holding down (freezing) $1s\,2s\,2p$ (Method 1) appears to have worked very well for Cu $K\alpha$, it has failed for Cu $K\beta$ (Table II). This is similar to the technique employed by Pham *et al.* [9], with the exception that we did not manually select the CSFs to be used here. Our purpose here is to demonstrate that false convergence occurs when an unoptimized technique is used, even if that technique was reasonably valid for another similar calculation. In this particular case, the only difference between Cu $K\beta$ and Cu $K\alpha$ is the "final" state where $K\alpha$

TABLE III. Copper $K\beta$ diagram lines using Method 2, where the $1s$ and $3p$ subshells are held inactive. Eigenvalues are more stable compared with Method 1. Gauges are also much more consistent and converged better. The change in energy between each iteration is also consistent across all transitions, unlike the results of $K\alpha$ at the $4f$ level. Almost 142 000 CSFs were used by the $5g$ level when using Method 2.

	Single configuration		Expansion to $4f$		Expansion to $5s$		Expansion to $5f$		Expansion to $5g$	
Transitions	Energy (eV)	A^L/A^V	Energy (eV)	A^L/A^V	Energy (eV)	A^L/A^V	Energy (eV)	A^L/A^V	Energy (eV)	A^L/A^V
$K\beta_1$										
$J=0\rightarrow J=1$	8902.76	1.0062	8902.09 (±0.67)	1.0061	8901.62 (±0.47)	1.0060	8902.28 (±0.66)	1.0061	8902.40 (±0.12)	1.0061
$J=1\rightarrow J=1$	8902.67	1.0063	8901.99 (±0.68)	1.0061	8901.51 (±0.48)	1.0060	8902.17 (±0.66)	1.0062	8902.29 (±0.12)	1.0062
$J=1\rightarrow J=2$	8902.92	1.0063	8902.20 (±0.72)	1.0061	8901.73 (±0.47)	1.0060	8902.38 (±0.65)	1.0062	8902.51 (±0.13)	1.0062
$K\beta_3$										
$J=0\rightarrow J=1$	8900.31	1.0065	8899.64 (±0.67)	1.0063	8899.18 (±0.46)	1.0062	8899.84 (±0.66)	1.0064	8899.97 (±0.13)	1.0064
$J=1\rightarrow J=0$	8900.36	1.0066	8899.66 (±0.70)	1.0064	8899.19 (±0.47)	1.0063	8899.85 (±0.66)	1.0065	8899.97 (±0.12)	1.0065
$J=1\rightarrow J=1$	8900.21	1.0066	8899.55 (±0.66)	1.0064	8899.07 (±0.48)	1.0063	8899.73 (±0.66)	1.0065	8899.85 (±0.12)	1.0065

has a hole at $2p$ while $K\beta$ has one at $3p$. On expansion to the multiconfiguration level $4f$, the convergence between the two gauges suffers dramatically, and the energies are clearly incorrect compared with the experimental Cu $K\beta$ spectra. Indeed, the single configuration result at the $4s$ level is preferred to the multiconfiguration result. Our wave function has been quite robust during the buildup of the copper atom using a single configuration method, but an erroneous application of multiconfiguration expansion can lead the entire calculation astray. Despite this gauge divergence between $4s$ and $4f$, they are still within less than 2% of one other. However, despite a relatively good degree of convergence between the gauges, the eigenvalues have converged poorly. Clearly, gauge convergence is a necessary but insufficient condition for assessing the quality of atomic calculations.

Table III summarizes the results of Method 2, where only the $1s$ and $3p$ subshells were frozen. Energies are well behaved compared with Method 1. The gauge convergence, at around 0.6%, is far superior and consistent at all levels. The changes in energy at each stage of expansion are consistent with each other, and the differences observed between $K\alpha_1$ and $K\alpha_2$ are not seen here between $K\beta_1$ and $K\beta_3$. However, the trend of convergence here is not monotonic, seen by the change in direction between $4f$, $5s$, and $5f$ multiconfiguration expansions. Results for both $K\alpha$ and $K\beta$ suggest that, at least *prima facie*, the best convergence might be obtained when the two subshells involved with the primary transition are kept inactive (frozen). In this case, the subshells to be kept inactive are $\{1s, 2p\}$ for $K\alpha$, and $\{1s, 3p\}$ for $K\beta$. In Method 1 of $K\beta$ when we replicated the technique of $K\alpha$, the $3p$ subshell

TABLE IV. Cu $K\beta$ diagram lines using Method 3 where we have held $1s\,2s\,2p\,3s\,3p$ fixed. Both energy and gauge convergence are excellent as we expanded to higher-order terms. Method 3 is more stable and robust than Method 2. Some transition eigenvalues are almost degenerate due to the rounding of the results, such as the case of $J=0\rightarrow 1$ and $J=1\rightarrow 0$ for $K\beta$ at the $6g$ level. Approximately 91 000 CSFs were used by the $6g$ level when using Method 3, which is considerably less than method 2 yet allows for higher-level expansion. The full spectrum expanded to $6g$ is included in text form in the Supplemental Material [33] as Kbicu-6g0.fcu-6g0.ct.

	Single configuration		Expansion to $4f$		Expansion to $5s$		Expansion to $5f$		Expansion to $5g$	
Transitions	Energy (eV)	A^L/A^V	Energy (eV)	A^L/A^V	Energy (eV)	A^L/A^V	Energy (eV)	A^L/A^V	Energy (eV)	A^L/A^V
$K\beta_1$										
$J=0\rightarrow J=1$	8902.76	1.0062	8903.04 (±0.28)	1.0063	8903.06 (±0.02)	1.0063	8903.44 (±0.38)	1.0064	8903.58 (±0.14)	1.0064
$J=1\rightarrow J=1$	8902.67	1.0063	8902.95 (±0.28)	1.0064	8902.96 (±0.01)	1.0064	8903.34 (±0.38)	1.0064	8903.48 (±0.14)	1.0065
$J=1\rightarrow J=2$	8902.92	1.0063	8903.15 (±0.23)	1.0063	8903.18 (±0.03)	1.0063	8903.52	1.0064	8903.66	1.0065
$K\beta_3$										
$J=0\rightarrow J=1$	8900.31	1.0065	8900.60 (±0.29)	1.0066	8900.62 (±0.02)	1.0066	8901.00 (±0.38)	1.0067	8901.15 (±0.15)	1.0067
$J=1\rightarrow J=0$	8900.36	1.0066	8900.62 (±0.26)	1.0066	8900.64 (±0.02)	1.0066	8901.00 (±0.36)	1.0067	8901.14 (±0.14)	1.0067
$J=1\rightarrow J=1$	8900.21	1.0066	8900.50 (±0.29)	1.0066	8900.52 (±0.02)	1.0066	8900.90 (±0.38)	1.0067	8901.04 (±0.14)	1.0068

	Expansion to $6s$		Expansion to $6g$		
$K\beta_1$					g_f
$J=0\rightarrow J=1$	8903.59 (±0.01)	1.0064	8903.61 (±0.02)	1.0064	0.0209132
$J=1\rightarrow J=1$	8903.49 (±0.01)	1.0065	8903.51 (±0.02)	1.0065	0.0131888
$J=1\rightarrow J=2$	8903.67 (±0.01)	1.0065	8903.70 (±0.03)	1.0065	0.0568483
$K\beta_3$					
$J=0\rightarrow J=1$	8901.15 (±0.00)	1.0067	8901.18 (±0.03)	1.0067	0.0134186
$J=1\rightarrow J=0$	8901.15 (±0.01)	1.0067	8901.18 (±0.03)	1.0067	0.0116048
$J=1\rightarrow J=1$	8901.05 (±0.01)	1.0068	8901.05 (±0.00)	1.0068	0.0213909

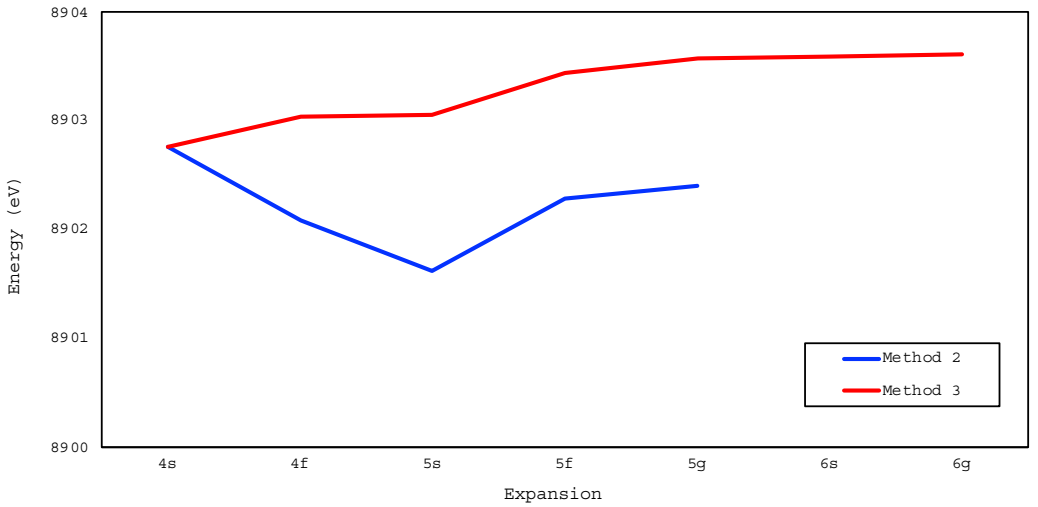

FIG. 2. A comparison of the Cu $K\beta_1(J = 0 \rightarrow J = 1)$ transition convergence for Methods 2 and 3. Both methods initially shift in opposite directions, but Method 2 (blue, lower line) changed course from the $5s$ level. Method 2 is less robust and stable than Method 3 (red, upper line). With further expansion, Method 2 should (we believe) eventually converge to the same results obtained using Method 3.

was left active, despite it being involved with the primary diagram transition, resulting in unsatisfactory outcomes. Using Method 2 resulted in over 166 000 CSFs by the $5g$ stage. This is unsurprising because there are more expansions than Method 1 (now up to $5g$ instead of $4f$) and there are also more active subshells (an addition of $2s$ and $2p$).

Table IV details copper $K\beta$ diagram lines using Method 3, acting as an analog of the technique used for $K\alpha$. While Method 2 appears to have worked well, it is quite novel. Our past experience suggests that having active subshells in between two layers of inactive ones can give rise to nonconvergence and even false convergence. In the case of Method 2, we have the active subshells of $2s\,2p\,3s$ bound between the inactive $1s$ and $3p$ subshells. For copper $K\alpha$, we purposely built up an atom with a frozen core that would encompass the two subshells that give rise to the primary diagram lines $(1s, 2p)$, along with everything in between, namely the $2s$ subshell. Doing the same thing for $K\beta$ would require the freezing of both $1s$ and $3p$, along with everything in between, which include $2s$, $2p$, and $3s$. Consequently, only the $3d$ and $4s$ subshells are active in the core copper atom. Hence, there are fewer active electrons to be excited into the higher-level subshells in order to generate higher-order terms to the atomic wave function, which allowed us to push the multiconfiguration computation to the $6g$ level.

The transition energies and gauges obtained using Method 3 appear to have converged well. From the $6s$ to the $6g$ expansion, the energies only changed by up to 0.02 or 0.03 eV.

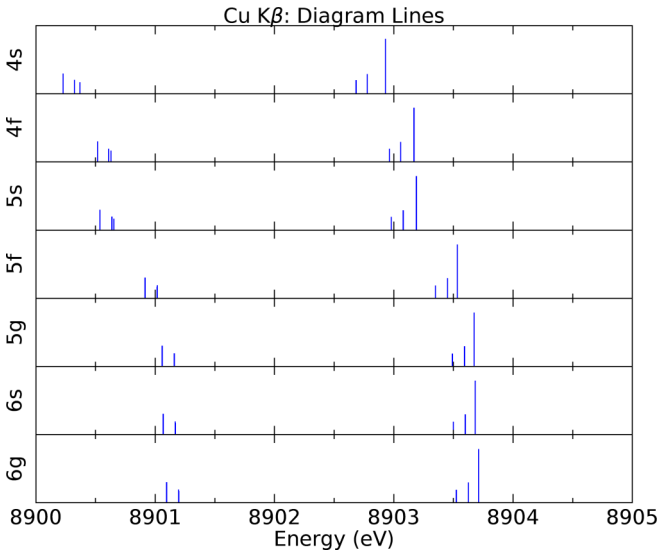

FIG. 3. Demonstration of the convergence of the eigenvalues of the Cu $K\beta$ diagram spectrum with expansion from single configuration $(4s)$ to outer orbitals $(6g)$.

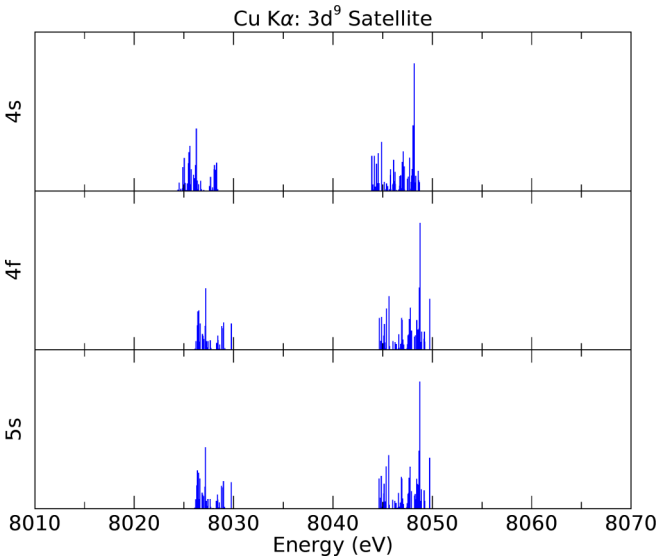

FIG. 4. Convergence of the eigenvalues of the dominant Cu $K\alpha$ $3d$-hole spectrum $(3d^9)$ with expansion to outer orbitals.

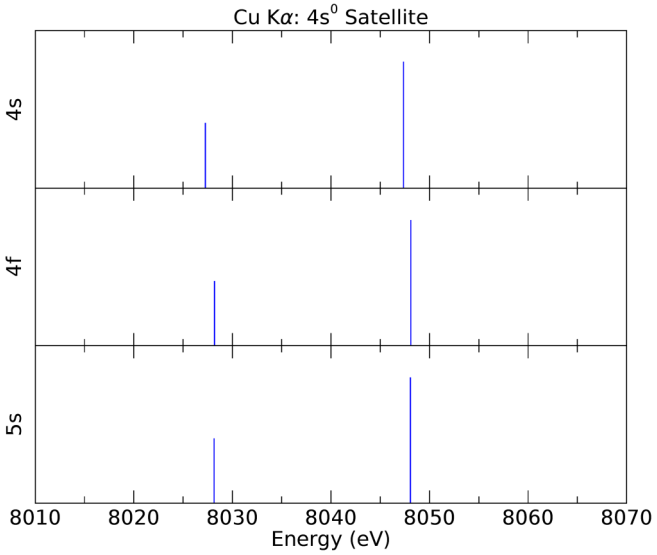

FIG. 5. Convergence of the Cu $K\alpha$ $4s$-hole spectrum ($4s^0$) with expansion to outer orbitals.

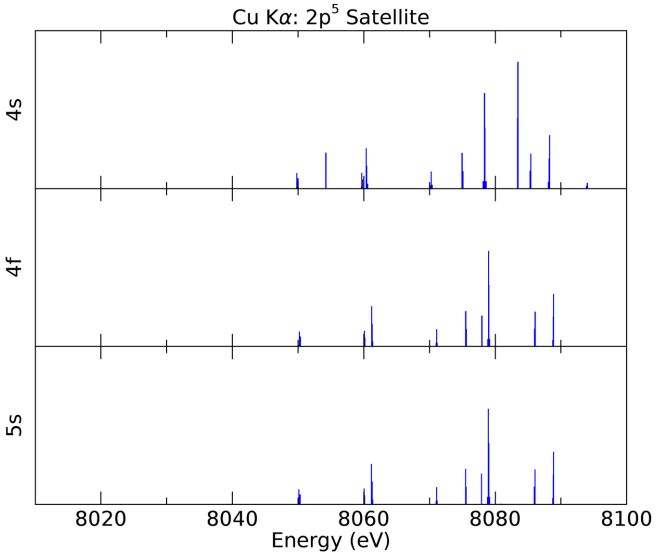

FIG. 7. Convergence of the Cu $K\alpha$ $2p$-hole spectrum ($2p^5$) with expansion to outer orbitals.

Such a small change between expansions is an indication that eigenvalues have converged, and that further expansion would not yield significant benefit. Results of Methods 2 and 3 may appear equally competitive in terms of quality and robustness, despite the differences in the eigenvalues. However, their trends show significant difference [Fig. 2, where we have used the $K\beta_1$ ($J = 0 \rightarrow J = 1$) transition for illustrative purposes—other transitions show a similar overall trend]. The two methods diverge from each other; then at the $5s$ expansion, Method 2 shows a reversal and the trend appears to converge towards Method 3. As Method 2 only had the $1s$ and $3p$ subshells inactive, expansion to $6s$ and $6g$ is computationally prohibitive due to the high number of active electrons. However, the expansion to $5g$ allows us to conclude that Method 3 is far superior than Method 2. Between the single configuration at the $4s$ level and the $6g$ multiconfiguration expansion, the energy changed by less than 1 eV for all the diagram transitions (see Fig. 3). This indicates that our wave functions are robust: less than 1 eV separates our single configuration solution from the more advanced multiconfiguration solution. By the $6g$ expansion, (only) about 78 000 CSFs were required using Method 3, compared with more than 140 000 using Method 2 to $5g$. Table IV also presents g_f using Method 3. On both stability and speed of computation, these results for Cu $K\alpha$ and $K\beta$ suggest that approaches analogous to Method 3 might be promising for other transition metals.

We find an intensity ratio $I(K\beta_3)/I(K\beta_1)$ of 0.510 33 after expansion to $6g$ (Table IV). Our ratio agrees very well with the theory of Pham *et al.* [9], reporting a ratio of 0.5107,

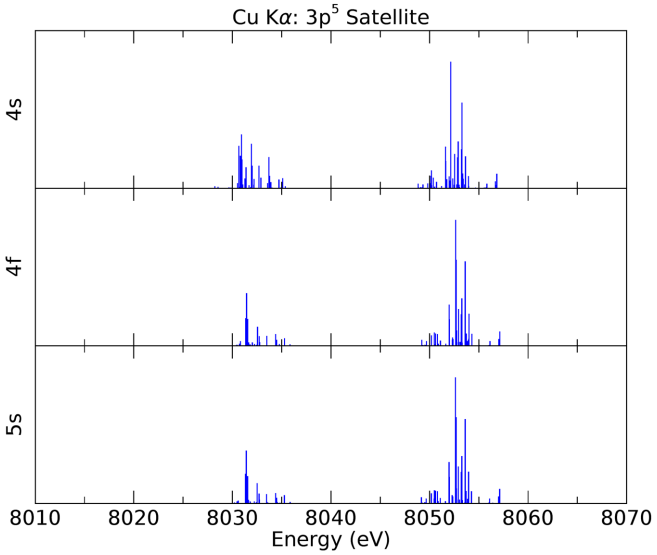

FIG. 6. Convergence of the Cu $K\alpha$ $3p$-hole spectrum ($3p^5$) with expansion to outer orbitals.

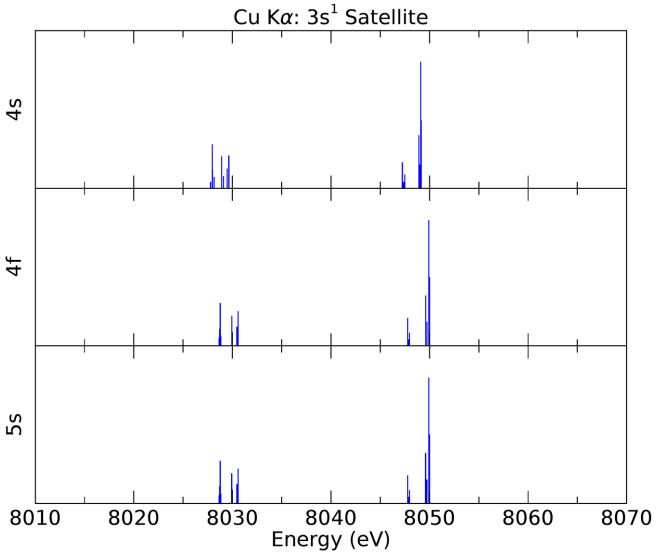

FIG. 8. Convergence of the Cu $K\alpha$ $3s$-hole spectrum ($3s^1$) with expansion to outer orbitals.

TABLE V. Convergence of the strongest $K\alpha$ transition for each of the satellite spectra. The energy and gauge convergence are excellent. With the exception of $3d^8$, all $K\alpha$ satellites were calculated using the same method as the diagram lines. The $4s^0$ satellite requires a very low number of CSFs, which makes it an ideal candidate for an approximation for the diagram line spectrum, as employed in previous studies [10]. Even with the restriction of the $3d$ subshell, the number of CSFs required to the $5s$ expansion (No. of CSFs) reaches 593 000. The number of eigenvalues for the satellite spectra range from 2 ($4s$ satellite) to 6 (diagram spectrum) to 1506 ($3d^8$ double shake). The full spectra expanded as indicated are included in text form in the Supplemental Material [33] as Kaicu3d9-5s.fcu3d9-5s.ct and similarly.

Copper $K\alpha$	Single configuration		Expansion to $4f$		Expansion to $5s$			
Satellite	Energy (eV)	A^L/A^V	Energy (eV)	A^L/A^V	Energy (eV)	A^L/A^V	No. of CSFs	No. of transitions
$3d^9$	8048.18	1.0069	8048.76 ± 0.58	1.0071	8048.73 ± 0.03	1.0070	258 000	131
$4s^0$	8047.36	1.0065	8048.10 ± 0.75	1.0067	8048.06 ± 0.04	1.0067	10 000	2
$3p^5$	8052.15	1.0072	8052.66 ± 0.51	1.0074	8052.64 ± 0.03	1.0073	185 000	102
$2p^5$	8083.45	1.0057	8079.17 ± 4.28	1.0042	8079.85 ± 0.68	1.0071	124 000	47
$3s^1$	8049.13	1.0066	8046.63 ± 2.50	1.0058	8046.77 ± 0.14	1.0059	59 000	19
$3d4s$	8048.47	1.0069	8049.08 ± 0.61	1.0071	8049.04 ± 0.04	1.0071	138 000	36
$3d^8$	8046.40	1.0066	8046.97 ± 0.57	1.0067	8046.94 ± 0.03	1.0067	593 000	1506

as well as Deutsch *et al.* [10], who reported a ratio of 0.51. Earlier theoretical work of Scofield [35] reported 0.511 for the diagram ratio, while Table 2 in [9] reports earlier experimental measurements of 0.5, 0.51, and 0.63. More recent work by Ito *et al.* [42] appears to state that the ratio is 0.596, which likely requires more rigorous examination. Omitting the anomalous extractions [42,43], these ratios for experiment and theory are in very good agreement, noting that experimental work will include satellites as well as the same difficulties mentioned above for $K\alpha$ ratios (see the Conclusion).

V. Cu $K\alpha$ CHARACTERISTIC EIGENVALUES AND AMPLITUDES: SATELLITE SPECTRA

Ab initio calculations of shakeoff satellite spectra for Cu $K\alpha$ are presented in Figs. 4–10. The methodology is as in the previous section, with the particular exception of the $3s^1$ satellite spectrum. This spectrum did not converge at the single configuration level using the basic $K\alpha$ characteristic expansion, which led to a collapse of the two distinct peaks into a single peak at an energy level that is about 50 eV above where the Cu $K\alpha$ peaks are expected. To overcome this issue, we kept the $3s$ subshell inactive for the $3s^1$ satellite calculation. Furthermore, the method of integration was changed to the nondefault "method 2" GRASP2K. The four different methods of integration available are relativistic versions of those described in [44]. Calculation for the $3d^8$ satellite (the $3d^2$ hole) required the suppression (freezing) of the $3d$ subshell; without such a constraint, the calculation for $3d^8$ at the $5s$ level would require in excess of 1 million CSFs.

There is a high level of convergence, and the theoretical (atomic) satellite spectra are well-defined. Calculations involving the $4s$ hole, namely the $K\alpha$ $4s^0$ satellite, require minor adjustments compared to the usual approach: As there is no electron in the $n = 4$ shell for this particular case, we have a complete open shell, rather than a partial open shell with the usual $4s^1$. Thus, the copper atom is treated as a closed-shell

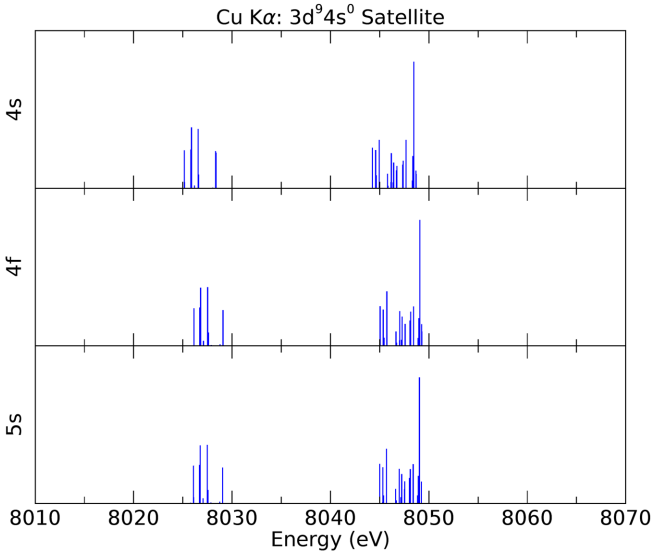

FIG. 9. Convergence of the dominant double shake Cu $K\alpha$ $3d4s$-hole spectrum ($3d^9 4s^0$).

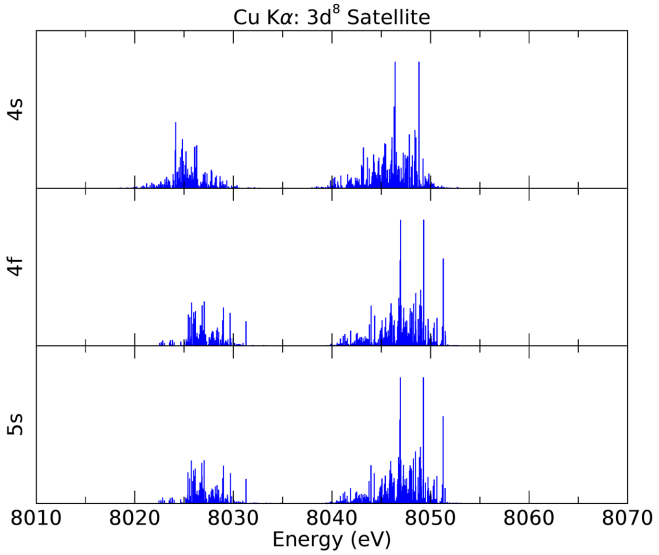

FIG. 10. Convergence of the internal double shake Cu $K\alpha$ $3d^2$-hole spectrum ($3d^8$).

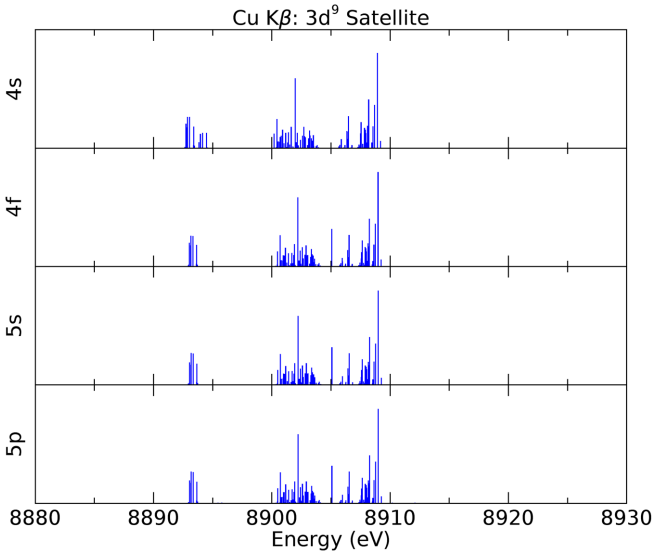

FIG. 11. Convergence of the eigenvalues of the dominant Cu $K\beta$ $3d$-hole spectrum ($3d^9$) with expansion to outer orbitals.

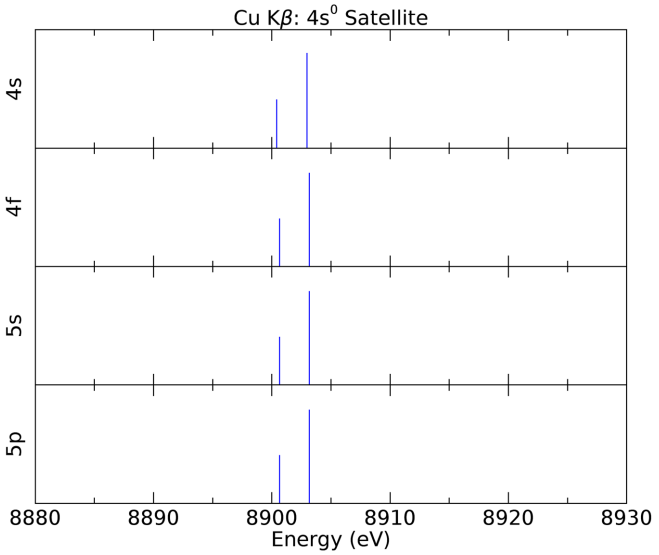

FIG. 12. Convergence of Cu $K\beta$ $4s$-hole spectrum ($4s^0$) with expansion to outer orbitals.

problem, with only two satellite transitions (Fig. 5). Removing the $4s$ electron has a relatively small effect on the spectra, as the satellite lines are located at almost exactly where the $K\alpha_1$ and $K\alpha_2$ should be. This is similar to approximations made in earlier work where the authors neglected the $4s$ electron in order to achieve convergence [10]. It explains why, despite that approximation, previous authors were able to achieve relatively good agreement with their experimental results. Detailed spectra are presented in the Supplemental Material [33] for the (converged) expansion to $5s$ orbitals. An anomaly in these results is the $2p$ satellite computation, where the most dominant transition at the single-configuration level appears to have shifted by about 4 eV at the multiconfiguration stage, whose intensity also decreased (Fig. 7). As such, the detailed spectra for $4s$, $4f$, and $5s$ expansions are given for the $K\alpha$ $2p$ satellite in the Supplemental Material [33] to aid further investigations. The relative intensities of satellite contributions are not defined by eigenvalue convergence or anomaly, but rather they are defined by the A-coefficients and g_f-values. From later sections it is expected, not just on the basis of degeneracy, that the $3d$-hole satellites are dominant. We present predicted and converged spectra for the two (dominant) double shakeoff spectra, namely $3d4s$ double hole and $3d^2$ double shakeoff. The significance of these two particular satellites is explained below. Table V provides a brief numerical summary of the satellite convergence where the strongest transition of each set is selected as representative of the entire group. Eigenenergies have converged to within less than an eV, and gauge ratios are virtually at unity by the $5s$ expansion.

VI. Cu $K\beta$ CHARACTERISTIC EIGENVALUES AND AMPLITUDES: SATELLITE SPECTRA

Figures 11–17 present theoretical shakeoff spectra for Cu $K\beta$. The expansion method is the same as for the diagram Cu $K\beta$ lines, where the subshells $1s\,2s\,2p\,3s\,3p$ were all kept inactive (Method 3). Hence, the number of CSFs required for these calculations is much lower than those used for $K\alpha$ satellite lines. Just under 4000 CSFs were required for the calculation of the $4s^0$ $K\beta$ satellite at the $5p$ level, compared with about 10 000 CSFs for $K\alpha$ at the $5s$ level. About 170 000 CSFs were required for the $K\beta$ $3d^8$ satellite at the $5p$ level compared with the $K\alpha$ $3d^8$ satellite, which required 593 000 CSFs. Convergence of all satellite spectra was smooth. Convergence issues observed with $K\alpha$ are likely due to the partially filled subshells of $3s$ and $3p$. There was no issue with the $3d$ satellites ($3d^9$ and $3d^8$), which are also partially filled: robust convergence was achieved without freezing the $3d$ subshell. Table VI provides the strongest transitions of the Cu $K\beta$ satellite lines, demonstrating numerical convergence. Energies of the $2p$ satellite transitions appear 60 eV

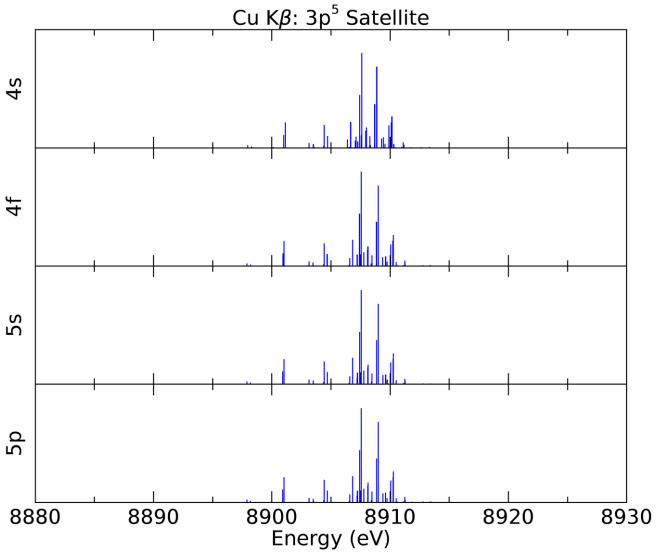

FIG. 13. Convergence of Cu $K\beta$ $3p$-hole spectrum ($3p^5$) with expansion to outer orbitals.

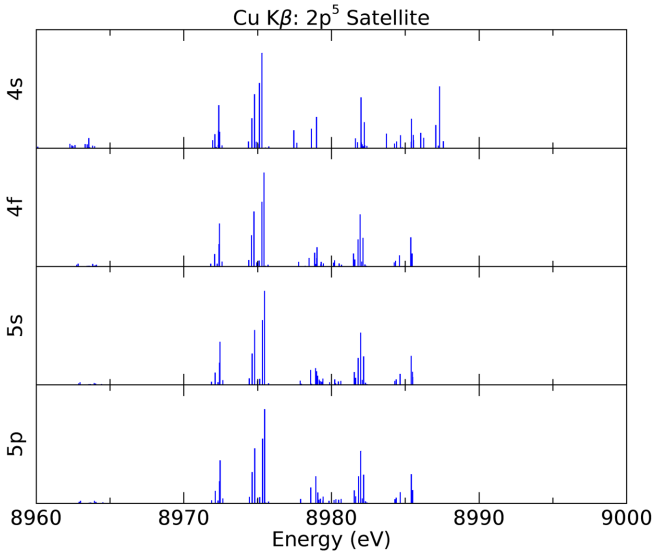

FIG. 14. Convergence of Cu $K\beta$ $2p$-hole spectrum ($2p^5$) with expansion to outer orbitals. These eigenvalues are significantly higher than the main spectrum.

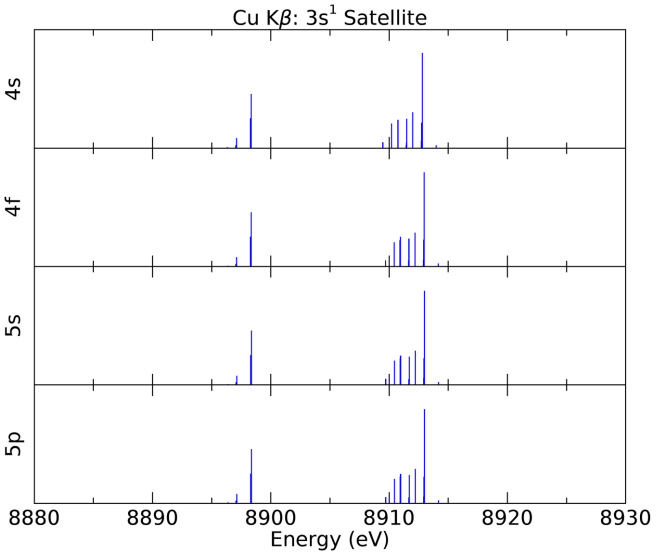

FIG. 15. Convergence of Cu $K\beta$ $3s$-hole spectrum ($3s^1$) with expansion to outer orbitals.

higher than other satellite spectra, approximately as expected (Fig. 14, Table VI). Curiously, this is located at around the same energy region where Ito *et al.* claim to have detected the Cu $K\beta_5$ peak [42]. Given the modest (relatively poor) level of gauge convergence for the $K\beta$ $2p^5$ satellite, it is possible that the $2p^5$ calculation has not converged completely.

VII. *AB INITIO* SHAKE CALCULATIONS

Ab initio calculations of shakeoff probabilities are calculated for each $n\kappa$ subshell: the probability of an electron from any one of these subshells being shaken off, following the photoionization event, but before the orbital relaxation. Following Eq. (20), the shake probabilities are extracted from the atomic wave functions at the ground (or neutral) state and immediately after the $1s$ electron has been removed. The shake probabilities should, in principle, be independent of whether the process is $K\alpha$ or $K\beta$ because they occur before the actual diagram transition in the sudden approximation limit. How should the wave functions $\phi_{Ajn\kappa}$ and $\phi_{Bkn\kappa}$ be constructed in order to apply Eq. (20)? This leads us back to our earlier premise—that there is no single method guaranteed to work for all situations. Hence, we have constructed the wave functions using two different methods: Method 1 (from $K\alpha$) and Method 3 (used for $K\beta$). Tables VII and VIII present shake probabilities calculated using these two methods of expansion.

Results at the single configuration level are unreliable and incomplete and thus should be disregarded, but they are included here for completeness. Method 1 is clearly not appropriate for a shake computation even though it works relatively well for Cu $K\alpha$ eigenenergies and satellites. The

TABLE VI. Convergence of the strongest $K\beta$ transition for each of the satellite spectra. These results have been obtained using Method 3 where we have held $1s\,2s\,2p\,3s\,3p$ fixed. The number of CSFs required at the $5p$ level was between approximately 4000 ($4s^0$) and about 170 000 ($3d^8$). For $3d4s$ extended to $6g$, *ca* 233 341 CSFs were used. The energy and gauge convergence are excellent as we expand to higher-order terms. The $2p^5$ satellite lines have relatively poor gauge convergence. The full spectra expanded as indicated are included in text form in the Supplemental Material [33] as Kbicu3d9-5p.fcu3d9-5p.ct and similarly. Two expansions are included for $3d4s$ given the discussion in the text.

	Single configuration		Expansion to $4f$		Expansion to $5s$		Expansion to $5p$			No. of
$K\beta$ Satellite	Energy (eV)	A^L/A^V	Energy (eV)	A^L/A^V	Energy (eV)	A^L/A^V	Energy (eV)	A^L/A^V	No. of CSFs	transitions
$3d^9$ satellite	8908.93	1.0074	8908.98 ± 0.06	1.0074	8909.00 ± 0.01	1.0074	8909.00 ± 0.001	1.0074	74699	131
$4s^0$ satellite	8902.97	1.0063	8903.18 ± 0.21	1.0063	8903.17 ± 0.01	1.0063	8903.18 ± 0.0005	1.0060	3986	2
$3p^5$ satellite	8907.60	1.0051	8907.56 ± 0.04	1.0051	8907.56 ± 0.01	1.0051	8907.57 ± 0.001	1.0051	55455	47
$3s^1$ satellite	8912.80	1.0082	8912.96 ± 0.16	1.0082	8912.99 ± 0.02	1.0082	8912.99 ± 0.003	1.0082	30320	19
$2p^5$ satellite	8975.29	0.8692	8975.43 ± 0.14	0.8692	8975.47 ± 0.04	0.8692	8975.47 ± 0.003	0.8692	125404	102
$3d4s$ satellite	8909.20	1.0074	8909.22 ± 0.02	1.0074	8909.22 ± 0.005	1.0074	8909.22 ± 0.001	1.0074		36
$3d^8$ satellite	8908.60	1.0069	8908.64 ± 0.05	1.0069	8908.65 ± 0.0104	1.0069	8908.65 ± 0.001	1.0069	169569	1506
	Expansion to $5g$		Expansion to $6s$		Expansion to $6g$					
$3d4s$ satellite	8909.41 ± 0.20	1.0075	8909.41 ± 0.0008	1.0075	8909.41 ± 0.000	1.0074			233341	36

TABLE VII. *Ab initio* shake probabilities for each $n\kappa$ subshell calculated at different levels of expansion using Method 1, where the $1s\,2s\,2p$ subshells were kept inactive. At the single configuration ($4s$) level, results are not sensible—higher-order terms are required. However, these shake probabilities appear to diverge as we expand to higher order.

Shake Probabilities (%)	$1s$	$2s$	$2p_{1/2}$	$2p_{3/2}$	$3s$	$3p_{1/2}$	$3p_{3/2}$	$3d_{3/2}$	$3d_{5/2}$	$4s$
Single config ($4s$)	−0.0641	−0.0037	0.1145	0.2157	0.155	0.354	0.361	1.351	1.405	8.827
$P_{n\kappa}$ expanded to $4f$	3.139	3.197	3.312	3.410	3.501	3.898	4.565	8.326	11.078	11.746
$P_{n\kappa}$ expanded to $5s$	3.580	3.638	3.752	3.849	3.940	4.335	4.999	8.743	11.483	12.147
$P_{n\kappa}$ expanded to $5f$	4.512	4.569	4.682	4.779	4.868	5.260	5.918	9.625	12.338	12.997
$P_{n\kappa}$ expanded to $6s$	4.867	4.924	5.037	5.133	5.222	5.612	6.267	9.961	12.664	13.320
$P_{n\kappa}$ expanded to $6d$	6.633	6.689	6.800	6.894	6.982	7.365	8.008	11.633	14.286	14.929

different methods of expansion dramatically affect the distribution of the mixing coefficients and hence the apparent shake probabilities. For the spectral calculations, we have achieved convergence via a number of metrics, such as low fluctuation of eigenenergy of the transition lines, as well as the relativistic gauge ratio reaching unity. The idea of convergence in the previous sections referred to the various outputs (energy, gauges, etc.) that are directly affected as the total atomic wave function was being changed, primarily through the addition of higher-order terms in the form of CSFs. For shake computations, even though we are adding more terms and changing the total wave function, the component of the wave function we are using to calculate the shake probabilities remains the same throughout all multiconfiguration stages. Hence $\phi_{Ajn\kappa}$ and $\phi_{Bkn\kappa}$ at the $4f$ level would look exactly the same as those at the $6g$ level, irrespective of how the multiconfiguration expansion was performed. The only difference is the distribution of the mixing coefficients. Irrespective of the method of expansion, the shake probabilities should be the same assuming that our wave function is complete. The converged shake probability results at the $6g$ expansion in Table VIII will therefore be used henceforth, unless stated otherwise.

After the departure from a single configuration at the $4s$ level, convergence is smooth and monotonic. The only large jump is at the transition from single configuration to multiconfiguration, i.e., between $4s$ and $4f$. Hence multiconfiguration results should be preferred over the single configuration results. Unsurprisingly, the $1s$ subshell has the lowest shakeoff probability among all the subshells due to the higher binding energy, whereas $3d$ and $4s$ are much more likely to be involved in shakeoff. The $3d$ shakeoff probability is among the largest satellite contributors to the copper $K\alpha$ spectrum. Many studies only investigate the $3d$ satellite (Table IX). Yet Table IX reveals that there is much disagreement between the various studies on the $3d$ shakeoff probability. Results from theoretical calculations have historically been lower than those of experiments. The extraction of satellite contributions from experimental spectra is nontrivial due to the overlapping transition energies displayed earlier. Therefore, experimental spectra are often analyzed through the broadening of theoretically calculated transition lines, which implicitly assumes that the theoretical calculations are accurate. Another reason for discrepancies between theory and experiment is that experiment generally fitted only the $3d$ satellite, rather than including other significant satellites. Consequently, this often artificially inflates the experimental estimate of the $3d$ satellite probability, and the experimental estimate is more representative of total shake probability, excluding the $4s$ probability, which is almost degenerate to the diagram lines. Theory has

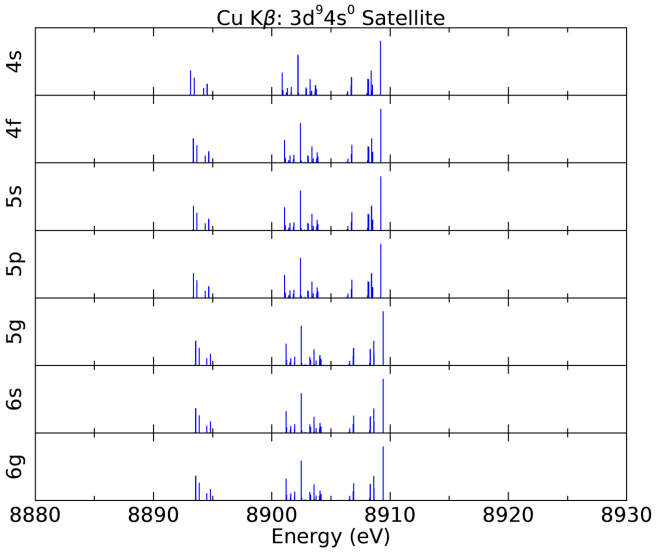

FIG. 16. Convergence of the dominant double shake Cu $K\beta$ $3d4s$-hole spectrum ($3d^9 4s^0$).

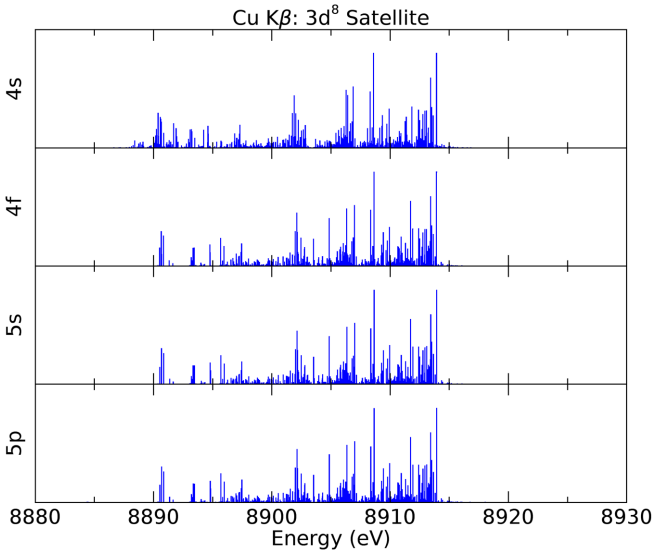

FIG. 17. Convergence of the internal double shake Cu $K\beta$ $3d^2$-hole spectrum ($3d^8$).

TABLE VIII. *Ab initio* shake probabilities for each $n\kappa$ subshell calculated at different levels of expansion using Method 3, where the $1s\,2s\,2p\,3s\,3p$ subshells were kept inactive. The shake probabilities converge well compared with Method 1 (Table VII).

Shake Probabilities (%)	$1s$	$2s$	$2p_{1/2}$	$2p_{3/2}$	$3s$	$3p_{1/2}$	$3p_{3/2}$	$3d_{3/2}$	$3d_{5/2}$	$4s$
Single config ($4s$)	−0.0641	−0.0037	0.1145	0.2157	0.155	0.354	0.361	1.351	1.405	8.827
$P_{n\kappa}$ expanded to $4f$	2.35667	2.4189	2.5332	2.6329	2.7275	3.1289	3.8084	7.5865	10.355	11.0336
$P_{n\kappa}$ expanded to $5s$	2.52667	2.5888	2.7029	2.8025	2.8969	3.2976	3.9759	7.7474	10.511	11.1885
$P_{n\kappa}$ expanded to $5f$	2.57725	2.6394	2.7534	2.8529	2.9473	3.3478	4.0257	7.7953	10.5575	11.2346
$P_{n\kappa}$ expanded to $6s$	2.57742	2.6395	2.7536	2.8531	2.9475	3.3479	4.0259	7.7954	10.5576	11.2347
$P_{n\kappa}$ expanded to $6g$	2.59898	2.6611	2.7751	2.8746	2.9689	3.3693	4.0471	7.8158	10.5774	11.2543
Total $P_{n\kappa}$ at $6g$	2.59898	2.6611	5.64964		2.9689	7.4164		18.3932		11.2543

been developing the determination of eigenvalues for diagram and satellite structure to this current work. Experimental fits of older spectral components and older experimental data are at least affected by (theoretical) spectral limitations in determination or convergence or the number of CSFs used or the expansion level, so they are generally less reliable.

All past theoretical predictions reported total shake probabilities as given in this table, whereas the experimental data will be dominated by individual satellite components, i.e., single shakeoff or double shakeoff probabilities. Results presented in this study are in relatively good agreement with the relativistic multiconfiguration work of Pham *et al.* [9]. A limitation of that work, however, is that all of the mixing coefficients were not utilized, nor were they properly normalized, which explains some significant differences in the results [9]. Table X demonstrates the importance of utilizing all the mixing coefficients and configurations. By not including all available terms, results can vary significantly. In the case of Pham *et al.*, the set of terms used for calculating shake probabilities was incomplete, and the terms were selected so that only the configurations with the largest contribution to the wave function were used. This inflated the probabilities and mismatched particular terms and their configurations, thus it misinterpreted and incorrectly applied Eq. (20). The other more complete set of results are those of Mukoyama and Taniguchi [29]. Their $4s$ result of 9.7% appears to be relatively close to our result of 11.25%. However, their work utilized a nonrelativistic single configuration method using Hartree-Fock-Slater wave functions, and interestingly it is quite close to our single-configuration result of 8.8% (at the $4s$ level). Discrepancies at the single configuration level, however, should be discounted as discussed.

VIII. SEPARATION OF SINGLE AND DOUBLE SHAKE ESTIMATES

$P_{n\kappa}$ gives us the probability of one or more electrons being removed from the $n\kappa$ subshell. We need to separate (isolate) single shake and double shake probabilities, especially since these correspond to markedly different satellite spectra. Double shake refers to when two electrons are ejected from the atom as a result of the change in the Hamiltonian when the initial $1s$ vacancy is created. The two electrons can either be removed from the same $n\kappa$ subshell, or from two different subshells. Calculating the probability of double shake from

TABLE IX. Theoretical and experimental shake probabilities for various satellite intensities in the literature. Experimental values have difficulty separating the components and are often empirical. Theoretical values to date have been total shake probabilities. †From Fig. 2 of [45]. ‡Normalised.

	Claimed Shake(off) Probabilities (%).						
Theory	$1s$	$2s$	$2p$	$3s$	$3p$	$3d$	$4s$
Mukoyama, Taniguchi (1987) [29]	0.003	0.097	0.456	0.34	2.5	9.7	9.7
Kochur *et al.* (2002) [45]					2.6	14.5	9.2†
Lowe *et al.* (2011) [16]						14.7	
Pham *et al.* (2016) [9]				0.32∓0.02	7.74∓0.10	19.94∓0.14	12.43∓0.15
This work (Total Shake to $6g$)	**2.60**	**2.66**	**5.65**	**2.97**	**7.42**	**18.39**	**11.25**
Experiment [extracting only P($3d$ shake)]							
Sauder *et al.* (1977) [14]						26.5±2‡	
Deutsch *et al.* (1995) [10]						26–30.0	
Hölzer *et al.* (1997) [36]						18.5	
Diamant *et al.* (2006) [32]						25±2	
Galambosi *et al.* (2003) [46]						25±2	
Enkisch *et al.* (2004) [47]						29.0	
Ito *et al.* (2006) [48]						23.1	
Chantler *et al.* (2009) [15]						29±2.5	
Chantler *et al.* (2010) [8]						26±1	
Chantler *et al.* (2012) [49]						15-30-39	

TABLE X. Total shake probabilities for subshells $3s$, $3p$, $3d$, and $4s$ based on the number of configurations. If only a finite number of configurations and mixing coefficients are used instead of utilizing all the mixing coefficients and configurations (as in Table VIII), then the terms must be ordered in terms of the dominant contribution to see the convergence. Convergence is specific to the level of expansion. The number of CSFs involved increases dramatically with expansion level so, e.g., 267 CSFs are required to *4f*; 311 to *5s*; 1530 to *5f*.

	Total Shake Probabilities $P_{n\kappa}$ (%)			
Number of configurations used	$3s$	$3p$	$3d$	$4s$
100	2.68	6.68	17.86	10.99
200	2.80	7.08	18.10	11.11
300	2.82	7.12	18.14	11.13
All (3543 at $6g$)	2.97	7.42	18.39	11.25

the same subshell is analogous to probability without replacement. Assuming that each of the $M_{n\kappa}$ electrons in a subshell is equally likely to be ejected as a result of the change in Hamiltonian, we can use binomial probability to calculate the probability of single and double shake. $P_{n\kappa}$ is the probability of at least one electron being removed from the $n\kappa$ subshell; in previous work, this has been incorrectly interpreted as the probability of a single electron being removed from the $n\kappa$ subshell and the other $M_{n\kappa} - 1$ remaining [9]. The importance of this was raised by Sachenko and Demekhin [27], though it was not clarified. If the probability of a success is given by p, then the probability of k successes out of n trials is

$$P(X = k) = \binom{n}{k} p^k (1-p)^{n-k}. \tag{26}$$

The probability of at least one success is the complement:

$$P(X \geqslant 1) = 1 - P(X = 0) = 1 - (1-p)^n, \tag{27}$$

$$p = 1 - (1 - P(X \geqslant 1))^{1/n}. \tag{28}$$

Substituting this into Eq. (26) and noting $P(X \geqslant 1) = P_{n\kappa}^{\text{shakeoff}}$ gives the probability of removing any k electrons out of a total of $M_{n\kappa}$ present in the subshell,

$$P(X = k) = \binom{M_{n\kappa}}{k} \left(1 - \left(1 - P_{n\kappa}^{\text{shakeoff}}\right)^{\frac{1}{M_{n\kappa}}}\right)^k \times \left(1 - P_{n\kappa}^{\text{shakeoff}}\right)^{\frac{M_{n\kappa}-k}{M_{n\kappa}}}. \tag{29}$$

The single and double shakeoff probabilities using Eq. (29) are shown in Table XI. The $3d4s$ shake probability is obtained by multiplying the probability of $3d$ and $4s$, giving 1.99%. For total double shake calculations, a cross-term was included to account for the possibility of electrons coming from subshells with the same n but different κ, e.g., one electron from $3p_{1/2}$ and one from $3p_{3/2}$, instead of both electrons coming from the same $n\kappa$ subshell.

The probability of two outer shell electrons being removed from the system during the initial $1s$ bombardment has been shown to be significant [9,25,45]. For copper, the $3d^2$ double shake structure has been calculated and applied when modeling the spectra in empirical fits [9,10]. Our calculated $3d^2$ double shake, 1.473%, is smaller than $1.79\% \mp 0.04$ reported by Pham *et al.* [9]. Although Pham *et al.* was fully relativistic, high-accuracy, and multiconfigurational, only a partial set of these high-accuracy results was used to estimate the shake probabilities. The authors selected only about 300 mixing coefficients and configurations with the largest contribution to the overall wave functions when applying the shake calculations. This slightly inflates the shake probabilities because the smaller contributions cancel out some dominant configurations. As the double shake calculation follows from the single shake calculations, the results from double shake were also slightly inflated. Herein we include all configurations, including the smaller ones.

The probability of a double shake due to a $4s$ and $3d$ electron ($3d4s$) is 1.99%. The $3d4s$ satellite spectral amplitude has not yet been extracted from experiment. Kochur *et al.* [45] provides an *ab initio* probability for the $3d4s$ double hole state in Cu to be 1.3%. There is significant overlap between the $3d4s$ structure and the diagram lines, making it hard to extract experimentally.

Equation (21) made several approximations. Probabilities using Eq. (21) can be compared with the Taylor series expansion Eq. (14):

$$P_{n\kappa}^{\text{shake}} = 1 - \left| \sum_j c_j d_j (1 - \epsilon_{n\kappa})^{M_{n\kappa}} \right|^2 \approx 1 - \left| \sum_j c_j d_j (1 - M_{n\kappa}\epsilon_{n\kappa}) \right|^2. \tag{30}$$

TABLE XI. Single and double shake probabilities calculated using Eq. (29) from the $P_{n\kappa}$ expanded to $6g$. The double shake nl probabilities include a (dominant) cross-term to include the probability of one electron from each $3d$ subshell being removed. This corrects the single shake probabilities and also yields, e.g., $3d^2$ double shake probability of 1.473%, in good agreement with the earlier *Ansätzes* [9] but usually a little smaller.

	Shakeoff probabilities (%) using Eq. (29)									
n, κ	1, −1	2, −1	2,1	2, −2	3, −1	3,1	3, −2	3,2	3, −3	4, −1
jj-coupling terms	$1s_{1/2}$	$2s_{1/2}$	$2p_{1/2}$	$2p_{3/2}$	$3s_{1/2}$	$3p_{1/2}$	$3p_{3/2}$	$3d_{3/2}$	$3d_{5/2}$	$4s_{1/2}$
n, κ single shake	2.599	2.643	2.756	2.843	2.947	3.340	3.985	7.579	10.091	11.254
Total nl single shake	**2.599**	**2.643**	**5.599**		**2.947**	**7.325**		**17.670**		**11.254**
								$3d4s$		1.99
n, κ double shake	0	0.018	0.020	0.031	0.022	0.029	0.062	0.234	0.474	0
Total nl double shake	**0**	**0.018**	**0.129**		**0.022**	**0.224**		**1.473**		0

TABLE XII. Comparison of the nl double shake probabilities using Eq. (29) with multiconfiguration expansion up to $6g$ with the method of Kochur *et al.* [45] [Eqs. (35) and (34)].

	Double Shake %							
	$1s$	$2s$	$2p$	$3s$	$3p$	$3d$	$4s$	$3d4s$
Our method	0	0.018	0.129	0.022	0.224	1.473	0	1.99
Method of Kochur *et al.* [45]	0	0.030	0.240	0.040	0.360	1.840	0	2.46

This is then relatively similar to the nonrelativistic analog

$$P_{nl}^{\text{shake}} \approx 1 - |(1 - M_{nl}\epsilon_{nl})|^2 = 1 - |[1 - M_{nl}(1 - \langle\phi_{Bknl}|\phi_{Ajnl}\rangle)]|^2 \quad (31)$$

and

$$p_{nl} \approx \frac{1}{M_{nl}}(1 - |(1 - M_{nl}\epsilon_{nl})|^2) \simeq (1 - \langle\phi_{Bknl}|\phi_{Ajnl}\rangle^2), \quad P_{nl}^{\text{shake}} \approx M_{nl}\,p_{nl}, \quad (32)$$

which for a single CSF can be related to the probability of no-shake and given a relative probability for total shakeup and shakeoff from the nl subshell (with respect to the probability of initial single ionization) of

$$\frac{P_{nl}^{\text{shake}}}{P_{nl}^{\text{no-shake}}} \approx 1 - \left[1 - \left(\frac{1 - \langle\phi_{Bknl}|\phi_{Ajnl}\rangle^2}{\langle\phi_{Bknl}|\phi_{Ajnl}\rangle^2}\right)\right]^{M_{nl}} \simeq M_{nl}\left(\frac{1 - \langle\phi_{Bknl}|\phi_{Ajnl}\rangle^2}{\langle\phi_{Bknl}|\phi_{Ajnl}\rangle^2}\right) = M_{nl}\left(\frac{1}{\langle\phi_{Bknl}|\phi_{Ajnl}\rangle^2} - 1\right) \quad (33)$$

as suggested by Kochur *et al.* [45]. Equations (31), (32), and (33) are single-CSF, nonrelativistic, Taylor series first-order approximations to Eq. (30), which in turn is a Taylor series approximation to Eq. (21). This does not make a good approximation in the real situation of multiconfigurational CSFs, so we should instead use Eq. (21).

Most authors use similar logic to estimate the shake probability as the probability of finding the wave function *not* in the $1s$ hole state. The critical issue is how $\langle\Psi_B(N)|\tilde{\Psi}_A(N)\rangle$ is calculated and separated into subshells.

For double shake estimates, Kochur *et al.* [45] expand upon their single-electron relative shake probability with their Eqs. (3) and (4):

$$P(1e \text{ from } nl,\, 1e \text{ from } n'l') \equiv P_{nl,n'l'} = M_{nl}M_{n'l'}\,p_{nl}\,p_{n'l'} = P_{nl}P_{n'l'}, \quad (34)$$

$$P(2e \text{ from } nl) \equiv P_{nl,nl} = \tfrac{1}{2}M_{nl}(M_{nl} - 1)p_{nl}^2, \quad (35)$$

which can be recast relativistically as approximations:

$$P(1e \text{ from } n\kappa,\, 1e \text{ from } n'\kappa') \equiv P_{n\kappa,n'\kappa'} = M_{n\kappa}M_{n'\kappa'}\,p_{n\kappa}\,p_{n'\kappa'} = P_{n\kappa}P_{n'\kappa'}, \quad (36)$$

$$P(2e \text{ from } n\kappa) \equiv P_{n\kappa,n\kappa} = \tfrac{1}{2}M_{n\kappa}(M_{n\kappa} - 1)p_{n\kappa}^2. \quad (37)$$

That is, when considering double shake from two *different* subshells, $n\kappa$ and $n'\kappa'$, the probabilities are simply multiplied together. A limitation of Kochur *et al.* [45] is that they use the probability of at least one shake as if it were the single shake probability of a particular electron. Furthermore, although they cite Sachenko and Demekhin [27], who use the full binomial equation, Kochur *et al.* [45] omit the $(1 - p)^{N-2}$ factor. Because the Kochur *et al.* method misinterprets (or perhaps approximates) P_{nl} as the single shake probability, applying their method to our values for $P_{n\kappa}$ gives single and double shake probabilities that are always slightly larger than our predictions (Table XII).

IX. ISOLATING SINGLE SHAKEOFF AND DOUBLE SHAKEOFF PROCESSES

Equation (29) only gives information about the particular $n\kappa$ subshell involved, e.g., the probability of removing a single electron from the $4s$ shell is calculated as 11.254%. However, this says nothing about what has happened in the other $n\kappa$ subshells. It does not distinguish between *one electron being removed from the* $4s$ *shell and all other subshells remaining as they are* and *one electron being removed from the* $4s$ *shell and a second electron being removed from a separate* $n\kappa$ *subshell.* Table XI gives the probability of single or double shake occurring in each of the $n\kappa$ shells, yet these values include the probabilities of additional shakes occurring in other shells. We need the probability of a single shake from $n\kappa$ *while all other subshells remain unchanged* to use these *ab initio* probabilities to fit satellite spectra to experimental data. This can be obtained by multiplying the probability of shake occurring in the $n\kappa$ by shake *not* occurring in each of the nine other subshells. This changes predictions quite significantly when compared

TABLE XIII. The probabilities of a single electron being removed from a subshell and all other electrons, both within the subshell and in all other subshells, remaining as is.

	Isolated single shakeoff probability (%) at $6g$ expansion									
n, κ	1,−1	2,−1	2,1	2,−2	3,−1	3,1	3,−2	3, 2	3,−3	4,−1
Shake probability at $6g$	1.57	1.60	1.67	1.72	1.79	2.04	2.45	4.84	6.65	7.47
nl	$1s$	$2s$	$2p$		$3s$	$3p$		$3d$		$4s$
Shake probability at $6g$	1.57	1.60	3.39		1.79	4.49		11.49		7.47

TABLE XIV. The probabilities (%) of two electrons being removed from two specific subshells and all other electrons, both within the subshells and in all other subshells, remaining as is. The data are from the 6*g* level of multiconfiguration expansion. The bottom row and the last column give total double shake from the specified nκ subshell. Entries highlighted on the diagonal are double shakes from the same $n\kappa$ subshell, while other subshells remain as is. Entries that are off-diagonal are double-shake probabilities from two different $n\kappa$ subshells, while other subshells remain as is.

n,κ	$1,-1$	$2,-1$	2,1	$2,-2$	$3,-1$	3,1	$3,-2$	3, 2	$3,-3$	$4,-1$	**total**
$1,-1$	**0.0000**	0.0427	0.0446	0.0460	0.0477	0.0544	0.0653	0.1293	0.1774	0.1994	0.807
$2,-1$	0.0427	**0.0109**	0.0453	0.0468	0.0486	0.0553	0.0664	0.1315	0.1806	0.2029	0.831
2,1	0.0446	0.0453	**0.0118**	0.0489	0.0507	0.0577	0.0694	0.1373	0.1885	0.2118	0.866
$2,-2$	0.0460	0.0468	0.0489	**0.0189**	0.0524	0.0596	0.0716	0.1418	0.1946	0.2187	0.900
$3,-1$	0.0477	0.0486	0.0507	0.0524	**0.0136**	0.0619	0.0743	0.1471	0.2019	0.2269	0.925
3,1	0.0544	0.0553	0.0577	0.0596	0.0619	**0.0176**	0.0846	0.1675	0.2299	0.2583	1.047
$3,-2$	0.0653	0.0664	0.0694	0.0716	0.0743	0.0846	**0.0381**	0.2012	0.2761	0.3103	1.257
3,2	0.1293	0.1315	0.1373	0.1418	0.1471	0.1675	0.2012	**0.1494**	0.5467	0.6144	2.366
$3,-3$	0.1774	0.1806	0.1885	0.1946	0.2019	0.2299	0.2761	0.5467	**0.3126**	0.8432	3.152
$4,-1$	0.1994	0.2029	0.2118	0.2187	0.2269	0.2583	0.3103	0.6144	0.8432	**0.0000**	3.086
Total	0.807	0.831	0.866	0.900	0.925	1.047	1.257	2.366	3.152	3.086	

with the single shake probabilities using Eq. (29) in Table XI (Table XIII). The same can be done for the double shake probabilities. Table XIV gives the probability of any two electrons being removed and all others remaining as is. The results are from the 6*g* multiconfiguration expansion. The numbers highlighted in the diagonal are double shakes from the same n,κ subshell. The last row and column give the total double shake from the specified subshell. For example, 3.086% is the total probability of a double shake involving the 4*s* electron, all else being equal. Notice that these reduced probabilities effectively also separate shakeup processes. For example, the probability of $3d4s$ double shake is 1.99% (see Table XII), however the probability of this occurring *while all other subshells remain unchanged,* $3d4s$ *only* is 1.4576% (0.6144 + 0.8432). The value 0.6144 is the probability of a double shake from the $n,\kappa = 3, 2$ ($3d_{3/2}$) and $n,\kappa = 4, -1$ ($4s_{1/2}$) subshells, while all other subshells remain unchanged. Similarly, the value 0.8432 is the probability of a double shake occurring from the $n,\kappa = 3, -3$ ($3d_{5/2}$) and $n,\kappa = 4, -1$ ($4s_{1/2}$) subshells, while other subshells remain the same. This implies that the difference in the probabilities from the two tables accounts for changes in electronic configurations at other subshells due to the shakeoff process. Similarly, the probability of $3d^2$ *only* double shake (see Table XV) is 0.9087% compared with the probability of *at least* $3d^2$ double shake, which is 1.473%. All other individual shake processes are less than 1%, e.g., $3p4s$ is only 0.5686%. The trend and relative magnitude of the probabilities in Table XIV are consistent with earlier tables given the different quantities presented.

The full spectral eigenvalues of diagram lines and of all satellite spectra are expanded as indicated and included in text form in the Supplemental Material [33] as, e.g., Kaicu3d9-5s.fcu3d9-5s.ct and similarly. These data can be used independently to predict and represent theoretical profiles of the full experimental spectra under appropriate impact conditions.

X. CONCLUSION

The theoretical results reported here represent the most extensive and complete treatment of copper $K\alpha$ and $K\beta$ diagrams and satellite spectra. Using a highly advanced relativistic framework, we have calculated diagram and satellite spectra to an extremely high level of accuracy, often to ~0.03 eV and some 10 times more accurate than earlier work. Diagram spectra are expanded to 5*s* with simultaneous convergence of 28 000 configuration state functions (CSFs) ($K\alpha$) and to 6*g* with simultaneous convergence of 91 000 CSFs ($K\beta$). The challenges of theoretical resources are demonstrated. Some challenges are explained by the need to invoke biorthogonalization, developments of the active space approach, analysis of markers for theoretical convergence of eigenvalues, and the question of self-consistency for both $K\alpha$ and $K\beta$ spectra. We detail gauge, eigenvalue, and *A*-coefficient convergence.

Complete single and double shake probabilities were calculated based on the multiconfiguration framework where all the configuration state functions were utilised, which includes the correct interpretation of the role of the mixing coefficients. This is evident by the convergence of the probabilities as higher-order expansions were included, as well as results that are within appropriate ranges within the literature. In doing

TABLE XV. The probabilities of a double electron being removed from two subshells and all other electrons, both within the subshell and in all other subshells, remaining as is.

	Dominant isolated double shakeoff probability (%) at the 6*g* expansion									
nl	$3d4s$	$3d^2$	$3p3d$	$3p4s$	$3s3d$	$3s4s$	$3p^2$	$3s3p$	$2p3d$	$2p4s$
Shake probability at 6*g*	1.458	0.9087	0.8747	0.5686	0.3490	0.2269	0.1403	0.1362	0.6622	0.4305

so, we have also provided our interpretation of shake probabilities in the sudden approximation model. The Cu $K\alpha$ $3d^8$ double-shake satellite spectrum alone contains 1506 unique eigenvalues (transitions) and required simultaneous convergence of 593 000 CSFs. This not only led to the calculation of total shake probabilities for all the subshells of copper ranging from $1s$ to $4s$, but it also resulted in the separation of single and double shake processes, which correspond to distinct eigenvalue spectra and asymmetries. We present computations for isolated shake events. Portable spectral representations are provided in the Supplemental Material [33] and discussed in the text. The processes computed herein pertain directly to the plasma evolution of XFEL spectra [50,51]. Note that the rapid ionization events leading to hollow atoms, etc., are defined by sequential and collective ionization and cascade probabilities. Results herein should prove essential for future theoretical work and comparison with experimental results.

ACKNOWLEDGMENT

We acknowledge the Australian Research Council grant application DP210100795 for the research grant for this work.

[1] M. Hansson, G. Berg, and M. Isaksson, X-Ray Spectrosc. **37**, 37 (2008).
[2] V. Jonauskas, G. Gaigalas, and S.Kučas, At. Data. Nucl. Data Tables **98**, 19 (2012).
[3] C. T. Chantler, M. N. Kinnane, C.-H. Su, and J. A. Kimpton, Phys. Rev. A **73**, 012508 (2006).
[4] D. A. Bradley, P. Muthuvelu, R. Ellis, E. Green, D. Attenburrow, R. Barrett, K. Arkill, D. Colridge, and C. Winlove, Nucl. Instrum. Methods B **263**, 1 (2007).
[5] R. Cesareo, M. A. Rizzutto, A. Brunetti, and D. V. Rao, Nucl. Instrum. Methods B **267**, 2890 (2009).
[6] K. A. Weaver, J. Gelbord, and T. Yaqoob, Astrophys. J. **550**, 261 (2001).
[7] C. S. Reynolds and A. C. Fabian, Astrophys. J. **675**, 1048 (2008).
[8] C. T. Chantler, J. A. Lowe, and I. P. Grant, Phys. Rev. A **82**, 052505 (2010).
[9] T. L. H. Pham, T. V. B. Nguyen, J. A. Lowe, I. P. Grant, and C. T. Chantler, J. Phys. B **49**, 035601 (2016).
[10] M. Deutsch, G. Hölzer, J. Härtwig, J. Wolf, M. Fritsch, and E. Förster, Phys. Rev. A **51**, 283 (1995).
[11] M. Deutsch and M. Hart, Phys. Rev. B **26**, 5558 (1982).
[12] L. G. Parratt, Rev. Mod. Phys. **31**, 616 (1959).
[13] S. Doniach and M. Sunjic, J. Phys. C **3**, 285 (1970).
[14] W. C. Sauder, J. R. Huddle, J. D. Wilson, and R. E. Lavilla, Phys. Lett. A **63**, 313 (1977).
[15] C. T. Chantler, A. C. L. Hayward, and I. P. Grant, Phys. Rev. Lett. **103**, 123002 (2009).
[16] J. A. Lowe, C. T. Chantler, and I. P. Grant, Phys. Rev. A **83**, 060501(R) (2011).
[17] P. Jönsson, G. Gaigalas, J. Bieroń, C. Froese-Fischer, and I. P. Grant, Comput. Phys. Commun. **184**, 2197 (2013).
[18] T. V. B. Nguyen, J. A. Lowe, T. L. H. Pham, I. P. Grant, and C. T. Chantler, The modified GRASP2K package, '1.15,' available from https://www.ph.unimelb.edu.au/~chantler/opticshome/softwarepackagedownloads.html#GRASP2KRCISE (2015).
[19] J. A. Lowe, C. T. Chantler, and I. P. Grant, Radiat. Phys. Chem. **85**, 118 (2013).
[20] C. Y. Zhang, K. Wang, M. Godefroid, P. Jönsson, R. Si, and C. Y. Chen, Phys. Rev. A **101**, 032509 (2020).
[21] C. T. Chantler, T. V. B. Nguyen, J. A. Lowe, and I. P. Grant, Phys. Rev. A **90**, 062504 (2014).
[22] G. Gaigalas and Z. Rudzikas, J. Phys. B **29**, 3303 (1996).
[23] G. Gaigalas, Z. Rudzikas, and C. Froese Fischer, J. Phys. B **30**, 3747 (1997).
[24] C. T. Chantler, T. V. B. Nguyen, J. A. Lowe, and I. P. Grant, Astrophys. J. **769**, 84 (2013).
[25] A. G. Kochur and V. A. Popov, J. Phys. B **39**, 3335 (2006).
[26] I. P. Grant, *Relativistic Quantum Theory of Atoms and Molecules—Theory and Computation*, 1st ed. (Springer Science and Business Media, New York, 2007).
[27] V. P. Sachenko and V. F. Demekhin, Sov. Phys. JETP **22**, 532 (1966).
[28] T. A. Carlson, C. W. Nestor, T. C. Tucker, and F. B. Malik, Phys. Rev. **169**, 27 (1968).
[29] T. Mukoyama and K. Taniguchi, Phys. Rev. A **36**, 693 (1987).
[30] M. Deutsch, O. Gang, K. Hämäläinen, and C. C. Kao, Phys. Rev. Lett. **76**, 2424 (1996).
[31] M. Fritsch, C. C. Kao, K. Hämäläinen, O. Gang, E. Forster, and M. Deutsch, Phys. Rev. A **57**, 1686 (1998).
[32] R. Diamant, S. Huotari, K. Hämäläinen, R. Sharon, C. C. Kao, and M. Deutsch, Radiat. Phys. Chem. **75**, 1434 (2006).
[33] See Supplemental Material at http://link.aps.org/supplemental/10.1103/PhysRevA.105.022811 for the full spectral eigenvalues of diagram lines and of all satellite spectra.
[34] E. Tiesinga, P. J. Mohr, D. B. Newell, and B. N. Taylor, J. Phys. Chem. Ref. Data **50**, 033105 (2021).
[35] J. Scofield, Phys. Rev. A **9**, 1041 (1974).
[36] G. Hölzer, M. Fritsch, M. Deutsch, F. Härtwig, and E. Förster, Phys. Rev. A **56**, 4554 (1997).
[37] M. H. Mendenhall, A. Henins, L. T. Hudson, C. I. Szabo, D. Windover, and J. P. Cline, J. Phys. B **50**, 115004 (2017).
[38] J. Williams, Phys. Rev. **44**, 146 (1933).
[39] S. I. Salem and R. J. Wimmer, Phys. Rev. A **2**, 1121 (1970).
[40] S. I. Salem, T. Falconer, and R. Winchell, Phys. Rev. A **6**, 2147 (1972).
[41] J. H. McGrary, L. V. Singman, L. H. Ziegler, L. D. Looney, C. M. Edmonds, and C. E. Harris, Phys. Rev. A **4**, 1745 (1971).
[42] Y. Ito, T. Tochio, M. Yamashita, S. Fukushima, A. M. Vlaicu, L. Syrocki, K. Słabkowska, E. Weder, M. Polasik, K. Sawicka, P. Indelicato, J. P. Marques, J. M. Sampaio, M. Guerra, J. P. Santos, and F. Parente, Phys. Rev. A **97**, 052505 (2018).
[43] H. H. Madden, D. M. Zehner, and J. R. Noonan, Phys. Rev. B **17**, 3074 (1978).
[44] C. Froese-Fischer, Comput. Phys. Rep. **3**, 273 (1986).
[45] A. G. Kochur, A. I. Dudenko, and D. Petrini, J. Phys. B **35**, 395 (2002).

[46] S. Galambosi, H. Sutinen, A. Mattila, K. Hämäläinen, R. Sharon, C. C. Kao, and M. Deutsch, Phys. Rev. A **67**, 022510 (2003).

[47] H. Enkisch, C. Sternemann, M. Paulus, M. Volmer, and W. Schülke, Phys. Rev. A **70**, 022508 (2004).

[48] Y. Ito, T. Tochio, H. Oohashi, and A. Vlaicu, Radiat. Phys. Chem. **75**, 1534 (2006).

[49] C. T. Chantler, J. A. Lowe, and I. P. Grant, Phys. Rev. A **85**, 032513 (2012).

[50] J. Hoszowska, A. K. Kheifets, J.-C. Dousse, M. Berset, I. Bray, W. Cao, K. Fennane, Y. Kayser, M. Kavčič, J. Szlachetko, and M. Szlachetko, Phys. Rev. Lett. **102**, 073006 (2009).

[51] J. Hoszowska, J. Szlachetko, J.-C. Dousse, W. Błachucki, Y. Kayser, C. Milne, M. Pajek, S. Boutet, M. Messerschmidt, G. Williams *et al.*, J. Phys.: Conf. Ser. **635**, 102009 (2015).